# Metal-Organic Framework Catalysts for Solar Fuels: Light-Driven Conversion of Carbon Dioxide into Formic Acid

J. Canivet, F. Wisser

# Metal-Organic Framework Catalysts for Solar Fuels: Light-Driven Conversion of Carbon Dioxide into Formic Acid

*Jerome Canivet*[†,]* *and Florian M. Wisser*[‡‖,]*

[†] Univ. Lyon, Université Claude Bernard Lyon 1, CNRS, IRCELYON - UMR 5256, 2 Avenue Albert Einstein, 69626 Villeurbanne Cedex, France

[‡] Institute of Inorganic Chemistry, University of Regensburg, Universitätsstraße 31, 93040 Regensburg, Germany

[‖] Erlangen Center for Interface Research and Catalysis, Friedrich-Alexander-Universität Erlangen-Nürnberg, Egerlandstraße 3, 91058 Erlangen, Germany

**Abstract.** The direct conversion of carbon dioxide into formic acid as renewable feedstock for chemicals or as fuel using sunlight as sole energy source would provide a crucial step towards a more sustainable industrialized society. While crucial advances have been made using molecular catalyst, their heterogenization within porous framework can provide additional features resulting in enhanced efficiency. Thanks to their high affinity towards carbon dioxide and high versatility in composition, Metal-Organic Frameworks (MOF) already offered appealing opportunities for the design of photocatalysts active in the light-driven carbon dioxide reduction into formic acid. In this Spotlight, we look back on a decade of discovery and understanding in the light-driven MOF-catalyzed formic acid production form carbon dioxide leading to a 1000-fold enhancement

in productivity and, moreover, opening perspectives for the design of novel porous hybrid photoactive platforms.



## 1. Introduction

The direct transformation of small molecules into more valuable synthetic intermediates is of paramount importance especially dealing with carbon dioxide ($CO_2$) as a practical and costless C1 reservoir to increase the sustainability of chemical processes.[1] In our industrialized society, reducing both the carbon footprint of the human activity and the level of greenhouse gases in the atmosphere using photons as sole energy source appears as an highly desirable, impactful and environmentally friendly process.[2] In this sense, converting carbon dioxide produced from industry and transportations into fuel or combustible using sunlight is a change in paradigm by transforming one of the main causes of climate change into a renewable resource towards a more sustainable society.[3] Indeed, tremendous achievements have been reached for the $CO_2$ photoreduction towards CO, through an easily accessible 2 electrons reduction, and $CH_4$, through a more challenging 8

electrons reduction process.[4] Formic acid (HCOOH) is another accessible 2 electrons reduction product from $CO_2$ considered as a promising renewable feedstock for fine chemical syntheses.[5] Furthermore, the development of fuel cells based on formic acid as hydrogen storage molecule is emerging due to its easy transportability, high volumetric energy density and hydrogen content.[6–8] Thus the direct and efficient photoreduction of carbon dioxide into formic acid will give access to sunlight conversion into chemical and electrical energy in a virtuous carbon cycle.[9]

While finely tunable homogeneous catalysts already demonstrated the efficiency of this photoreduction process, the controlled heterogenization of well-defined single-site catalysts on various supports, such as carbon nitride, metal oxides or porous hybrids, is an appealing way to increase the sustainability of molecular catalytic processes by saving energy, with an easier catalyst isolation from the product, and precious resources, with an increased catalyst stability thanks to single-site isolation.[10–18] Beyond the advantageous easy separation of solubilized product from the solid catalyst and the possible recycling of the later, the heterogenization of a single-site molecular complex within a porous host allows to control the catalytic activity by the design of the host framework.[19]

Thanks to their hybrid organic-inorganic nature, Metal-Organic Frameworks (MOF), as platform for the heterogenization of single-site catalysts, allow to adjust structure-properties relationships from molecular design of the catalyst local environment towards the solid's surface interactions with both substrates and light.[20] Indeed, among other heterogeneous sytems,[21–24] MOF are highly promising carbon dioxide photoconversion candidates thanks to their tunable affinity with carbon dioxide and high storage capacity, their high versatility in composition as photoactive solid from either their organic or inorganic building units, their possible post-synthetic modification for introducing additional light harvesting unit and/or catalytic sites, and finally thanks to their ordered

network allowing the structuration of photosystems components to get long lasting excited states.[25–27]

Here we aim at reviewing a decade of discovery and advances in the ever-growing field of MOF photocatalysis while shining light towards formic acid production as sustainable energy vector, with a 1000-fold improvement in productivity (Table 1) since the first report on this topic. The increased sophistication in the design of multifunctional MOF frameworks and the subsequent structure-activity relationships open also perspectives for the development of other porous solid hybrid photocatalysts like porous organic polymers (POP) and metal-organic polyhedra (MOP).

In this article, the product of carbon dioxide reduction reaction is referred to as formic acid, as at least under the standard conditions used in most of the literature studies which are mixtures of acetonitrile and triethanolamine (Table 1), this amine is not basic enough to deprotonate formic acid, which may however not be the case under other conditions. Additionally, catalytic activities are always compared as the catalyst productivity $R$ defined as $R = \frac{n_{\text{formic acid}}}{m_{\text{solid}} \cdot t}$, with $n_{\text{formic acid}}$ the amount of formic acid produced in mmol, $m_{\text{solid}}$ the total amount of solid catalyst used in g and $t$ the reaction time in h. We used this nomenclature, as for some catalytic systems the precise nature of the active site is still under debate, avoiding the use of turnover frequencies or turnover numbers to compare catalysts. Indeed the comparison of the catalytic activity per gram of solid material has been stated to allow for direct comparison between different systems and reports.[28] However, as for homogeneous catalysis,[29,30] often precise information about the reactor design and the light source (position from the reactor, constant radiant flux or irradiance) are not reported, making the direct comparison of turnover numbers / frequencies or quantum efficiency, but also productivities between different research laboratories, challenging. Also, the reproducibility of photocatalytic experiments remains scarce, adding another challenge for reproducing and comparison of data.

Table 1. Overview over MOF-, POP- and MOP-based catalyst for $CO_2$ to HCOOH photoreduction.

| support | postulated catalyst | photosensitizer | *R* / mmol/h/g | *t* / h | conditions | ref. |
|---|---|---|---|---|---|---|
| Ti-MIL-125-$NH_2$ | Ti-O node | amino linker | 0.016 | 10 | ACN-TEOA, 500 W Xe lamp, λ > 420 nm | [31] |
| UiO-66-$NH_2$<br>UiO-66-$(NH_2)_2$ | Zr-O node | amino linker | 0.026<br>0.041 | 10 | ACN-TEOA, 500 W Xe lamp, λ > 420 nm | [32] |
| Zr-SDCA-$NH_2$ | Zr-O node and amino linker | amino linker | 0.096 | 12 | ACN-TEOA, 300 W Xe lamp, λ > 420 nm | [33] |
| UiO-66-$NH_2$<br>UiO-66 | leached Zr species | linker | 0.032<br>0.010 | 12 | ACN-TEOA, 5 : 1, 200 W Xe lamp | [34] |
| UiO-66-$NH_2$ | leached Zr species | linker | 0.056 | 12 | ACN-DEA, 5 : 1, 200 W Xe lamp | [34] |
| Fe-MIL-101-$NH_2$ | Fe-O node | amino linker | 0.448 | 8 | ACN-TEOA, 300 W Xe lamp, λ > 420 nm | [35] |
| Pt/Ti-MIL-125-$NH_2$ | Ti-O node | amino linker | 0.032 | 8 | ACN-TEOA, 300 W Xe lamp, λ > 420 nm | [36] |
| Ir1/A-UiO-66-$NH_2$<br>Ir1/Ti-MIL-125-$NH_2$ | Ir sites | amino linker | 0.51<br>0.27 | 10 | water-isopropanol, 300 W Xe lamp, λ > 420 nm | [37] |
| Ir1/A-UiO-66-$NH_2$ membrane | Ir sites | amino linker | 3.38 | | Gaseous $CO_2$ feed saturated with water vapours, 300 W Xe lamp, λ > 420 nm | |
| Cu NCs/UiO-66-$NH_2$ | Cu NCs | amino linker | 0.128 | 18 | DMAc-TEOA, 300 W Xe lamp, λ = 385 nm | [38] |

Table 1. Overview over MOF-, POP- and MOP-based catalyst for CO2 to HCOOH photoreduction. (Continued)

| Support | catalyst | photosensitizer | *R* / mmol/h/g | *t* / h | conditions | ref. |
|---|---|---|---|---|---|---|
| KGF-9 | not determined | thiadiazole linker | 1.15 | 5 | DMSO-BIH, LED, 370-500 nm | [39] |
| Ga-MFM-300 | not determined | not determined | 0.50 | 4 | ACN -TEOA, 300 W Xe lamp, 350-780 nm | [28] |
| Ir-CP | Ir site | Ir site | 0.119 | 6 | ACN-TEOA, 500 W Xe lamp, λ > 475 nm | [40] |
| Ru-MOF powder<br>Ru-MOF nanoflower | Ru site | Ru site | 0.031<br>0.077 | 8 | ACN-TEOA, 500 W Xe lamp, λ > 420 nm | [41] |
| UiO-66-catechol | $Cr^{3+}$<br>$Ga^{3+}$ | catechol linker | 1.72<br>0.56 | 6 | ACN -TEOA-BNAH, 300 W Xe lamp, λ > 420 nm | [42] |
| MOF-545-Fe<br>nano-MOF-545-Fe | Zr-O node | porphyrin linker | 0.57<br>1.52 | 4 | ACN-TEOA, 280 W Xe lamp, λ > 420 nm | [43] |
| In-TCP-Co<br>Fe-TCP-Co<br>In-TCP-OH-Co<br>Fe-TCP-OH-Co | In/Fe-catecholate node | porphyrin linker | 0.001<br>0.004<br>0.006<br>0.017 | 6 | water, 300 W Xe lamp, λ > 420 nm | [44] |
| Ni/Mg-MOF-74 | Ni/Mg-O node | $Ru(bpy)_3Cl_2$ | 0.53 | 0.5 | ACN -TEOA, 300 W Xe lamp, λ > 420 nm | [45] |

Table 1. Overview over MOF-, POP- and MOP-based catalyst for $CO_2$ to HCOOH photoreduction. (Continued)

| Support | catalyst | photosensitizer | *R* / mmol/h/g | *t* / h | conditions | ref. |
|---|---|---|---|---|---|---|
| CPP<br>HRh2-CPP<br>SAG | $C_{12}Rh_2$-CPP<br>HRh2-CPP<br>$C_{12}Rh_2$-SAG | $Ru(bpy)_3Cl_2$ | 58.6<br>75.7<br>53.7 | 2 | ACN-TEOA, ABA solar simulator | 46 |
| CPP<br>HRh2-CPP<br>SAG | $C_{12}Rh_2$-CPP<br>HRh2-CPP<br>$C_{12}Rh_2$-SAG | $Ru(bpy)_3Cl_2$ | 29.9<br>32.7<br>25.1 | 4 | ACN-TEOA, 200 W Xe lamp, λ > 420 nm | |
| UiO-67-bpy | Mn(CO) | $Ru(dmb)_3(PF_6)_2$ | 5.03 | 18 | DMF-TEOA-BNAH, LED, λ = 470 nm | 47 |
| UiO-67-bpy | Ru(terpy) | $Ru(bpy)_3Cl_2$ | 1.07 | 6 | ACN-TEOA, 300 W Xe lamp, λ = 385-740 nm | 48 |
| UiO-67-bpy | Cp*Rh(bpydc) | $Ru(bpy)_3Cl_2$ | 0.34 | 10 | ACN-TEOA, 200 W Xe lamp, λ > 420 nm | 49 |
| MIL-101-$NH_2$ | Cp*Rh(bpydc) | $Ru(bpy)_2(bpydc)Cl_2$ | 0.026 | 5 | ACN-TEOA, 280 W Xe lamp, λ > 425 nm | 50 |
| $PW_{12}$/Cp*Rh@UiO-67-bpy | Cp*Rh(bpydc) | $Ru(bpy)_3Cl_2$ | 0.52 | 3 | ACN-TEOA, 280 W Xe lamp, λ > 415 nm | 51 |
| MOF-253<br>BpyMP-1<br>BpyMP-1-$NH_2$ | Cp*Rh(bpy) | $Ru(bpy)_3Cl_2$ | 0.78<br>3.73<br>4.18 | 4 | ACN-TEOA, 200 W Xe lamp, λ > 420 nm | 52 |

## 2. MOF photocatalysts with pure organic linkers

In the following examples, the MOF described are themselves light sensitive and photoactive for the reduction of carbon dioxide without use of any external photosensitizer or catalyst, mainly thanks to light harvesting amino-functionalized linkers and catalytic metal-oxo nodes.

### 2.1 (Ti/Zr/Fe) amino-MOF

In the case of amino-functionalized linkers, the strategy takes advantage of the light harvesting properties of the amino-functionalized linker and ability for transfer charges towards the inorganic node acting as catalyst for the $CO_2$ transformation.

Among the first example of MOF-catalyzed $CO_2$ photoreduction towards HCOOH, Li and coworkers reported the use of Ti-MIL-125-$NH_2$ as efficient photocatalyst (Figure 1).[31] This Ti-based MOF is made from titanium oxo-cluster linked by 2-amioterephthalate linkers, formulated as $Ti_8O_8(OH)_4(bdc\text{-}NH_2)_6$ (bdc-$NH_2$ = 2-amino-benzene-1,4-dicarboxylate). Being highly porous towards nitrogen with an apparent surface area of 1300 $m^2/g$, Ti-MIL-125-$NH_2$ show superior $CO_2$ adsorption uptake with 132 $cm^3/g$ at 273 K compared to its non-functionalized parent Ti-MIL-125 with an uptake of 99 $cm^3/g$. More importantly, the absorbance is shifted into the visible region, the absorption edge is around 550 nm. The strong absorbance in the visible part of the spectrum has been attributed to an O to Ti ligand to metal charge transfer (LMCT) in the $TiO_5(OH)$ cluster. For the photocatalytic reduction of $CO_2$, the Ti-MIL-125-$NH_2$ was suspended into a $CO_2$-saturated acetonitrile solution using triethanolamine (TEOA) as electron donor in a 5:1 volume by volume ratio and irradiated using a Xe lamp equipped with filters to produce light in the range 420-800 nm. Under these conditions the productivity reached 0.016 $mmol_{HCOOH}/g_{cat}/h$ and isotope labelling experiment using $^{13}CO_2$ confirmed that $CO_2$ was the unique source of HCOOH. As for other $TiO_2$ related photocatalyst,[53,54] a photochromic behavior (color transition from yellow to green) was

observed upon light excitation and in the presence of an electron donor and under exclusion of $O_2$ and $CO_2$. Combining UV Vis and electron spin resonance (ESR) spectroscopy, the authors attributed the color change to intervalence electron transfer from Ti(III) to Ti(IV) sites in the titanium oxo-clusters. The Ti(III) sites are supposed to be generated by a long-lived excited charge separation state also occurs by transferring a photo excited electron from bdc-$NH_2$ linker to Ti(IV) site. The linker is reductively quenched by electron transfer from TEOA, while the Ti(III) sites are stable under $N_2$ atmosphere (Figure 1).

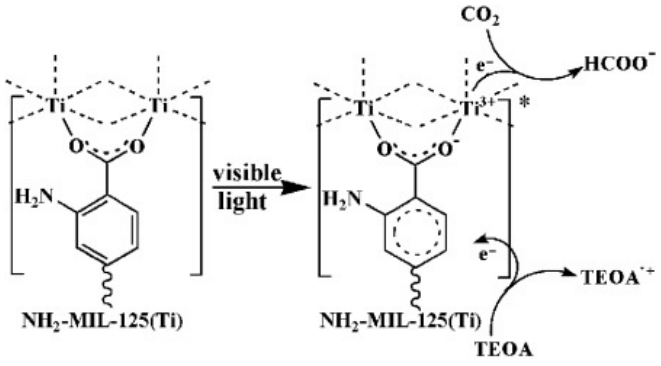


Figure 1. Postulated mechanism for the light-induced $CO_2$ reduction catalyzed by Ti-MIL-125-$NH_2$. Reprinted with permission from reference 31. Copyright 2012 WILEY-VCH Verlag GmbH & Co. KGaA, Weinheim.

Following a similar methodology, the same group studied Zr-based MOF analogue as photocatalyst candidates for $CO_2$ photoreduction.[32] They reported in this study the UiO-66-$NH_2$ composed of hexameric $[Zr_6O_4(OH)_4]^{12+}$ units linked by bdc-$NH_2$ and formulated as $Zr_6O_4(OH)_4$(bdc-$NH_2$)$_6$. Similar to previous reports, the substitution of the organic terephthalate linker in UiO-66 by bdc-$NH_2$ results in the visible-light-responsive UiO-66-$NH_2$. The photocatalytic $CO_2$ reduction was performed under the exact same conditions the productivity reached 0.026 $mmol_{HCOOH}/g_{cat}/h$. Combining photoluminescence (PL) and ESR spectroscopy the authors speculated that a similar mechanism than in Ti-MOF occurred, involving bdc-$NH_2$ as

photosensitizer and charge transfer to potential $Zr^{3+}/Zr^{4+}$ at the MOF node. However, the precise mechanism and in particular the occurrence of a LMCT and the role of the node or leached Zr species as catalytic active centers is still under debate (see below).[34,43] Furthermore, the authors took advantage of the high stability and high versatility of UiO MOF to partly substituted bdc-$NH_2$ in UiO-66-$NH_2$ by 2,5-diaminoterephthalic acid (bdc-$(NH_2)_2$) to obtain an aminated UiO-type MOF with mixed bdc-$NH_2$ and bdc-$(NH_2)_2$ linkers. The mixed-linker aminated UiO-66 presented similar textural properties than its analogues with a slightly higher $CO_2$ uptake. Diffuse-reflectance UV/Vis spectroscopy showed also a stronger absorption in the visible region than for pure mono-aminated UiO-66-$NH_2$. Under the same catalytic conditions, the amount of HCOOH formed reached about 20.7 µmol in 10 h (0.041 $mmol_{HCOOH}/g_{cat}/h$), more than 50% higher than over the mono-aminated UiO-66-$NH_2$. The improved photocatalytic performance was attributed to the enhanced light absorption and $CO_2$ adsorption resulting from the tuning of MOF's linker properties thanks to additional functional group, here the second amino group.[55] Another variation around diamino-functionalized UiO-type MOF was more recently reported by Xing and coworkers.[33] They combined amino-functionalized conjugated linker (2,2′-diamino-4,4′-stilbenedicarboxylic acid, $H_2$SDCA-$NH_2$) with $ZrCl_4$ to prepare a novel UiO-type MOF named as Zr-SDCA-$NH_2$ (Figure 2). Being isoreticular to UiO-type MOF with the fcu topology, the Zr-SDCA-$NH_2$ has the same framework structure as UBMOF-8[56] with an apparent surface area of 2550 $m^2/g$. Notably, Zr-SDCA-$NH_2$ presents a strong absorption band between 400–600 nm. The Zr-SDCA-$NH_2$ photocatalyst allowed to reach the production of 18.8 µmol of HCOOH after 12 hours of continuous visible light irradiation, corresponding to a productivity of 0.096 $mmol_{HCOOH}/g_{cat}/h$. Importantly, the activity of the $H_2$SDCA-$NH_2$ linker alone in solution reached 19.6 µmol in 12 h, 29 mg linker (0.097 mmol; 16.8 µmol/h/mmol linker) when aminoterephthalic acid was found to

be inactive in $CO_2$ photoreduction under the same conditions. According to UV-Vis and PL studies, two parallel pathways were postulated to take place within the MOF photocatalyst. As found for other aminated MOF, the SDCA-$NH_2$ can act as light harvesting unit which transfer charges to $Zr_6O_4(OH)_4(COOR)_{12}$ cluster though ligand-to-metal-charge-transfer (LMCT) process, the $CO_2$ transformation taking place at Zr-O sites, but the SDCA-$NH_2$ linker could also directly react with $CO_2$ to generate HCOOH upon excitation.

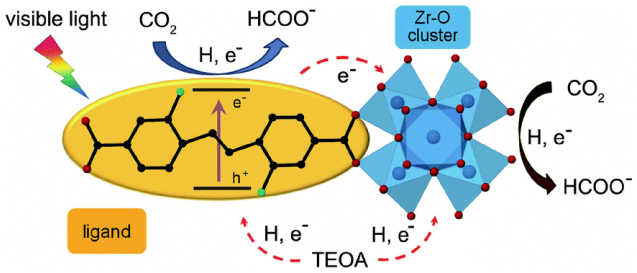


Figure 2. Postulated mechanism for the light-induced $CO_2$ reduction catalyzed by SDCA-$NH_2$. Reprinted with permission from reference 33 with permission from the Royal Society of Chemistry.

However, the precise mechanism of all Zr-based catalysts is still under debate and the role of leached species requires careful consideration. Saouma and co-workers observed for series of UiO-66 type catalysts with varying functionalization of the linker or particle size that an important parameter to be considered is the amount of Zr leached during the photocatalysis under basic conditions. In their study they considered TEOA or diethylamine (DEA) as sacrificial electron donor.[34] To stimulate the leaching that may occur under photocatalytic conditions, they suspended the UiO-66-$NH_2$ catalysts in an ACN/electron donor suspension for 24h under $N_2$ atmosphere. Afterwards, the particles were separated from the supernatant and redispersed in a fresh solution of electron donor in ACN. Both, the supernatant (~0.1 to 0.3 % of Zr leached) and the pre-treated MOF catalyst were then used in photochemical $CO_2$ reduction reaction. The authors observed a

much higher HCOOH productivity over the leached Zr species than over the MOF, indicating that the leached species are catalytically active. As during catalysis with the MOF, Zr leaching still occurred, a clear statement on the catalytic activity of the nodes in the MOF could not be given. Separation of the supernatant and the spent MOF catalyst showed that also the species leached during catalysis are catalytically active in a second cycle. The precise nature of the leached Zr species is still under investigation. Similarly, the amount of HCOOH produced increased with increasing amount of leached Zr species within a series of UiO-66-$NH_2$ MOFs. Note that, when the production of HCOOH is normalized to the mass of MOF used and the reaction time, very similar apparent activities were observed as for other studies using the same MOF (Table 1).[32] However, when also other parameters such as the functionalization of the bdc-linker were changed, no direct correlation between leached amount of Zr and catalytic activity could be given. Another important observation made by Saouma and co-workers is that for DEA as sacrificial electron donor a constant and stable evolution of HCOOH over the course of the reaction was observed. In contrast, for TEOA as sacrificial electron donor the catalytic activity levels off after a few hours, in line with other reports in literature. Thus, for most UiO-66 derivatives investigated, the use of DEA as sacrificial electron donor yields higher HCOOH concentrations.

Extending the series of amino-MOF, Li and coworkers studied iron-based MOF series with different topologies, namely Fe-MIL-101-$NH_2$, Fe-MIL-53-$NH_2$ and Fe-MIL-88B-$NH_2$.[35] Fe-MIL-101-$NH_2$ has a three-dimensional crystal structure and is formed of octahedral trimeric iron (III) clusters linked by 2-aminoterephthalate linkers generating two types of mesoporous quasi-spherical cages of 29 Å and 34 Å diameter. In Fe-MIL-53-$NH_2$, chains of iron (III) centered corner-sharing octahedra, joined along the chain through hydroxyl oxygens, are linked perpendicular to the chains to four chains by 2-aminoterephthalate linkers, thus generating one-dimensional flexible

diamond-type channels of 3.5 to 8 Å diameter. Fe-MIL-88B-$NH_2$ is made of trimeric Fe(III) shared by $\mu_3$-O and linked by 2-aminoterephthalate linkers giving access to flexible three-dimensional cages with diameter form 6 to 16 Å. As found in the case of Ti and Zr-based amino-MOF, the amino-functionalized Fe-based MOF materials show enhanced absorption in the visible light region compared to non-aminated parents. Also, amino-functionalized MOFs show enhanced activity for photocatalytic $CO_2$ reduction. The best catalyst reported, Fe-MIL-101-$NH_2$, allowed reaching productivity of 0.45 $mmol_{HCOOH}/g_{cat}/h$ in acetonitrile/TEAO mixture using a 300 W Xe lamp (400-800 nm). A reported 3-fold productivity enhancement from Fe-MIL-101 to aminated analogue was attributed to a postulated synergy between two photocatalytic pathways (Figure 3). Indeed, in addition to the direct excitation of FeO cluster, a second pathway, similar to other amino-MOF photocatalysts, considered the excitation of the amino linker followed by charge transfer from the excited linker to the metal node.

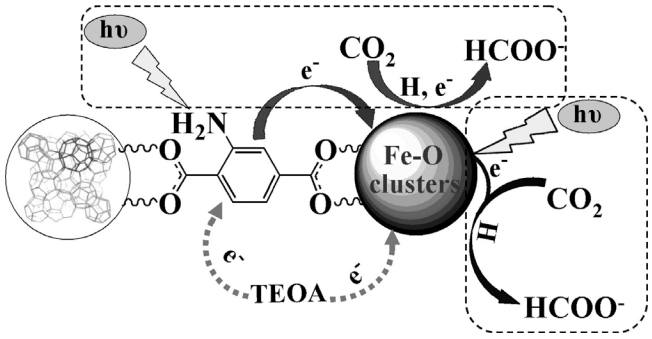


Figure 3. Postulated synergetic reaction mechanism for the light-induced $CO_2$ reduction catalyzed by Fe-MIL-101-$NH_2$. Reproduced from Wang et al. *ACS Catal.* **2014**, *4* (12), 4254–4260.[35] Copyright 2014 American Chemical Society.

## 2.2 Doping amino-MOF with transition metals

Li and coworkers also demonstrated that doping Ti-MIL-125-$NH_2$, using either $[PtH_2Cl_6] \cdot 6\ H_2O$ or $[AuHCl_4] \cdot 4\ H_2O$ as precursor, affect the catalytic activity of the MOF in the photocatalytic $CO_2$ reduction.[36] After impregnation and reduction, the Pt and Au were found in the MOF both as isolated atoms, clusters and small nanoparticles of 30 Å and 25 Å, respectively, with however an ill-defined location. Under the same conditions than those used for Ti-MIL-125-$NH_2$, Au doping in Au/Ti-MIL-125-$NH_2$ induced a slight decrease in HCOOH acid production as well as a significant production of $H_2$, not reported for Ti-MIL-125-$NH_2$. In contrast, Pt/Ti-MIL-125-$NH_2$ shows an important production of $H_2$ of 0.58 $mmol_{H2}/g_{cat}/h$ and a slight increase in HCOOH production to 0.032 $mmol_{HCOOH}/g_{cat}/h$ (compared to 0.025 $mmol_{HCOOH}/g_{cat}/h$ using pure Ti-MIL-125-$NH_2$). This increase in activity for both water and $CO_2$ visible light-driven reduction was attributed to hydrogen spillover from Pt particles to bridging oxygen linking Ti sites, thus favoring the formation of $Ti^{3+}$ active species.

Wang and coworkers also studied the effect of amino-MOF doping, UiO-66-$NH_2$, by impregnation with Ir salt inside defective MOF.[37] The design of defective UiO MOF, named A-UiO-66-$NH_2$, is based on the missing linkers approach, leading to accessible hydroxyls site on the $Zr_6O_4(OH)_4(COOR)_{12}$ node to which Ir atoms are grafted using $K_2IrCl_6$ precursor. Iridium isolated atoms (Ir1) were found highly dispersed in the UiO-66-$NH_2$ after annealing with loadings of 0.7 wt%. Extended X-ray absorption fine structure (EXAFS) analysis evidenced Ir–O bonds with an average coordination number of 3.8 and the absence of Ir–Ir bonds confirming the isolated characters of the Ir atoms. For higher loadings, (ca. 1.4 to 2.7wt%) the formation of small Ir clusters was also reported. The Ir1/A-UiO-66-$NH_2$ served as the photocatalyst for the $CO_2$ reduction. The authors followed the same methodology using Pd atoms for $O_2$ reduction reaction. In a

water/isopropanol mixture under irradiation of a 300W Xe lamp equipped with a 420 nm long-pass filter, the Ir1/A-UiO-66-$NH_2$ produced HCOOH with a rate of 0.24 $mmol_{HCOOH}/g_{cat}/h$ with a high selectivity of 96.3%, with $H_2$ being the only by-product. Increasing the iridium loading to 1.4 wt% boosted the HCOOH productivity to 0.51 $mmol_{HCOOH}/g_{cat}/h$ with a near full selectivity. The difference in activity was attributed to difference in electronic structure between isolated atoms and clusters. As revealed by X-ray absorption near-edge structure (XANES) and X-ray photoelectron spectroscopy (XPS) analysis, Ir atoms were more positively charged than Ir clusters and particles. A two-steps mechanism for the production of HCOOH was postulated involving $CO_2$ adsorption at the MOF's surface, generating carbonate species, followed by hydrogenation at Ir site using photogenerated electrons provided by the excited amino-MOF and protons from water. The authors also showed a similar trend for Ir single atoms on Ti-MIL-125-$NH_2$, with an increase from 0.013 $mmol_{HCOOH}/g_{cat}/h$ (same range than Li and coworkers[31,36]) to 0.27 $mmol_{HCOOH}/g_{cat}/h$ for pristine Ti-MIL-125-$NH_2$ and Ir-doped Ti-MIL-125-$NH_2$, respectively. Finally, the Ir1/A-UiO-66-$NH_2$ particles were deposited as a membrane onto commercially available porous poly-tetrafluoroethylene (PTFE) films following a layer-by-layer protocol.[37] By shaping the MOF catalyst as a membrane, they showed that $CO_2$ adsorption was facilitated and the contact between the gaseous $CO_2$ and the catalytic sites was enhanced. Importantly the use of a gaseous feeds allowed to use only water vapor as proton and electron donor, thus avoiding the need of any sacrificial electron donor. Indeed Ir1/A-UiO-66-$NH_2$ membrane was found to catalyze the $CO_2$-to-HCOOH photoreduction with productivity of 3.38 $mmol_{HCOOH}/g_{cat}/h$, largely surpassing the activity of the analogous powder catalyst. However, the crucial effect of the MOF support nature, including the topology and node composition, remained elusive.

More recently, Serre and coworkers incorporate ultrasmall Cu nanocrystals (Cu NCs, diameter 1.6 nm) into two Zr-MOFs, MOF-801 (also called Zr-fumarate) and UiO-66-$NH_2$ (Figure 4),[38] their strategy is based on growing the MOF shell around pre-synthesized Cu NCs. The Cu NCs@UiO-66-$NH_2$ composite showed similar crystallinity and porosity as the pristine UiO-66-$NH_2$, with a loading of 2.85 at% of Cu as determined by ICP-MS. TEM analysis of the Cu NCs@MOF-801 and Cu NCs@UiO-66-$NH_2$ composites show a decent distribution of ultrasmall Cu nanocrystals within the MOF. The $CO_2$ photoreduction experiments were carried out using TEOA as a sacrificial electron donor under UV irradiation (385 nm) at room temperature for 18 h. The Cu NCs@MOF-801 was found to produce mainly CO (22.5%) and HCOOH (64.9%) with rates of 0.032 $mmol_{CO}/g_{cat}/h$ and 0.094 $mmol_{HCOOH}/g_{cat}/h$, respectively. In contrast, Cu NCs@UiO-66-$NH_2$ showed an enhanced reactivity for HCOOH production with a rate of 0.128 $mmol_{HCOOH}/g_{cat}/h$. This enhancement was attributed to a higher affinity of UiO-66-$NH_2$ for $CO_2$ as evidenced by $CO_2$ sorption isotherm measurements. Other by-products (methanol, CO and formaldehyde) were observed in low amounts, their production being comparable for both catalysts.

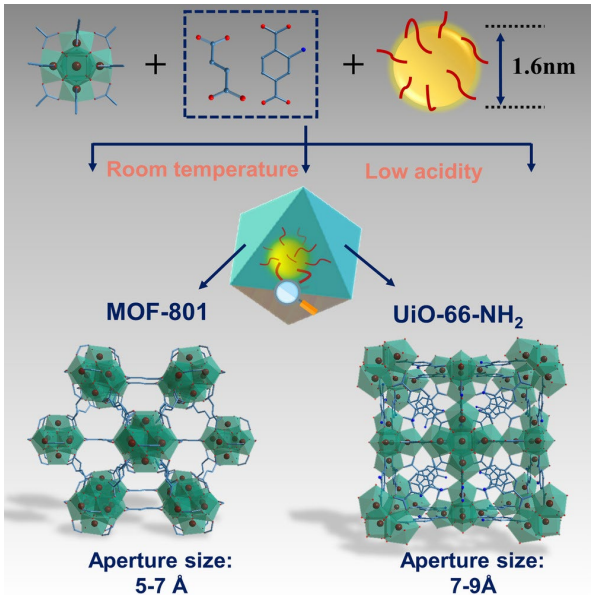

Figure 4. Synthesis of Cu NCs@MOF composites as $CO_2$ photoreduction catalysts under UV irradiation. Reprinted with permission from reference 38. Copyright 2022 WILEY-VCH Verlag GmbH & Co. KGaA, Weinheim.

### 2.3 Non-aminated MOF

**PbS-Coordination Polymers.** Tanaka, Maeda and coworkers reported the $CO_2$ photoreduction using non-porous coordination polymer (CP) made with $Pb^{2+}$ cations linked by 1,3,4-thiadiazole-2,5-dithiol, named KGF-9, and containing $(-Pb-S-)_n$ infinite structure.[39] KGF-9 presented a very small surface area of 0.7 $m^2/g$. Using a solution of 1,3-dimethyl-2-phenyl-2,3-dihydro-1*H*-benzo[*d*]imidazole (BIH) in dimethylsulfoxide (DMSO) under 370−500 nm light irradiation, KGF-9 allowed reaching a HCOOH productivity of 1.15 $mmol_{HCOOH}/g_{cat}/h$. XPS measurements revealed that part of the surface linker was decomposed during catalysis but KGF-9 largely maintained its framework structure. Although the reaction mechanism of $CO_2$ reduction by KGF-9 still remained to be elucidated, it represents the first example of Pb-promoted $CO_2$ reduction.

**Ga-MFM-300.** Very recently, Schröder, Yang and coworkers reported a Ga-based MOF photocatalyst.[28] Ga-MFM-300 was made of $[GaO_4(OH)_2]_n$ chains linked by biphenyl-3,3′,5,5′-tetracarboxylates and showed an apparent surface area of 1060 $m^2/g$ and a $CO_2$ uptake of 5 mmol/g at 298 K and 1 bar. In a $CO_2$-saturated acetonitrile solution containing triethanolamine under irradiation at 350–780 nm the photoreduction of $CO_2$ over Ga-MFM-300 produced HCOOH with a productivity of 0.5 $mmol_{HCOOH}/g_{cat}/h$ and excellent selectivity and stability. The activity of Ga-MFM-300 was attributed to the ability of bridging OH sites within the pore to bind and activate $CO_2$ followed by the generation of $CO_2^{\bullet-}$ radical anions intermediate as postulated based on electron paramagnetic resonance spectra of trapped radical intermediates (Figure 5).

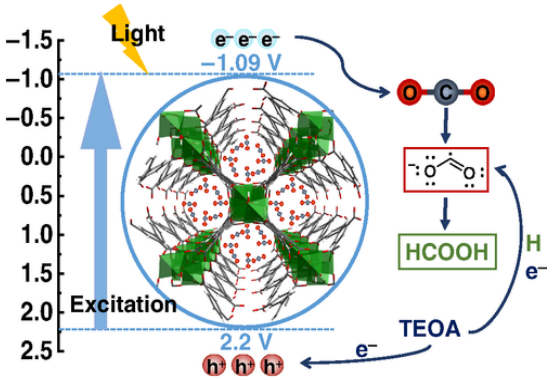


Figure 5. Light-driven $CO_2$ photoreduction catalyzed by Ga-MFM-300. Reprinted with permission from reference 28 with permission from the Chinese Chemical Society (CCS).

## 3. MOF with photocatalytic metalolinker

In this section, the MOF were synthesized using metalolinker to be all-in-one photocatalyst where the inorganic nodes acted mostly as structuring agent. The metalolinker being a well-defined molecular photocatalyst, the heterogenous MOF-catalyzed carbon dioxide photoreduction proceeded without any external photosensitizer.

### 3.1 Iridium and ruthenium polypyridyl linkers

Luo and coworkers reported an Y-based coordination polymer (CP) using $Ir(ppy)_2(dcbpy)$ (ppy : 2-phenylpyridine, dcbpy : 2,2′-bipyridine-4,4′-dicarboxylate as metalolinker.[40] The Ir-CP solid was made by chains of hydroxy-bridged Y(III) linked by two $Ir(ppy)_2(dcbpy)$ metalolinkers. The neighboring chains packed with each other through π- π interactions to form a three-dimensional supramolecular framework. The Ir-CP was not found porous but its light adsorption range was found to be the same than that of the isolated Ir unit. In an acetonitrile-triethanolamine mixture

under visible-light irradiation (Xe lamp with filter) the Ir-CP was found to produce HCOOH with a rate up to 0.119 $mmol_{HCOOH}/g_{cat}/h$. The Ir-CP was reported to be recyclable for up to five runs with however a slight decrease I productivity and an observable leaching of Ir of 3% after one catalytic run. The Ir-Cp was found more stable than its homogeneous $Ir(ppy)_2(H_2dcbpy)$ counterpart. This superiority was attributed to the structuration of Ir sites within CP framework with increased rigidity, resulting also in longer-lived excited states.

Later, the same group described light-harvesting Ru-MOF made by combination of $Ru(H_2dcbpy)_3$ linker (dcbpy : 2,2′-bipyridine-4,4′-dicarboxylate) and cadmium perchlorate (Figure 6).[41] This Ru-MOF, formulated as $\{Cd_2[Ru(dcbpy)_3] \cdot 12\ H_2O\}_n$, resulted in a six-connected pcu network structure. Moreover, the authors showed that Ru-MOF was easily tuned from sub-millimeter scale flakes to micro-scale flakes (about 10–30 μm) and nanoflowers. In an acetonitrile-triethanolamine mixture under visible-light irradiation (Xe lamp with filters 420–800 nm) the Ru-MOF was found to produce HCOOH with a rate up to 0.077 $mmol_{HCOOH}/g_{cat}/h$, being stable and recyclable. Comparing the Ru-MOF with its constitutive molecular Ru units, the luminescence lifetime of the Ru-MOF was more than one order of magnitude higher than that of the molecular Ru complex. The longer luminescence and thus excited-state lifetime have been stated to be crucial for an efficient photocatalytic process. The authors also demonstrated the advantage of three-dimensional hierarchical nanostructured crystals with increase productivity found for nanoflowers compared to micro-flakes and bulk crystals (respectively 0.077, 0.053 and 0.031 $mmol_{HCOOH}/g_{cat}/h$). The superior efficiency of Ru-MOF nanoflowers was attributed to their larger surface-to-volume ratio compared to bulk crystals as well as their high energy transfer efficiency, indicated by the highest quantum yield observed for the nanoflowers in the series.

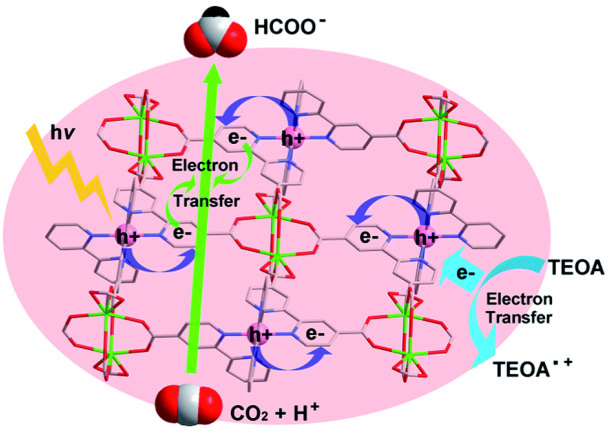


Figure 6. Postulated mechanism for the light-driven $CO_2$ photoreduction catalyzed by Ru-MOF. Reprinted with permission from reference 41 with permission from the Royal Society of Chemistry.

### 3.2 Metalated catecholate linker

Cohen and coworkers reported chromium and gallium catecholate derivatives as linker in the UiO-66 framework (Figure 7).[42] The Zr-based MOF was subjected to post-synthetic linker exchange with 2,3-dihydroxyterephthalic acid ($H_2$catbdc) to produce UiO-66-CAT which was metalated at the catechol site using $Cr^{3+}$ or $Ga^{3+}$ salts. XPS analysis of the as-prepared UiO-66-CrCAT and UiO-66-GaCAT confirmed the trivalent oxidation state of Cr and Ga in the MOFs. In this case, the catbdc organic linkers were responsible for visible light absorption and the metalation by $Cr^{3+}$ and $Ga^{3+}$ was found to facilitate the electron transfers within the MOFs. Using a mixed solution of TEOA and 1-benzyl-1,4-dihydronicotinamide (BNAH, 0.1 M) in acetonitrile under visible light irradiation (300 W Xe arc lamp equipped with cut-off filters 420-800 nm), the HCOOH productivity of UiO-66-CrCAT and UiO-66-GaCAT reached 1.72 $mmol_{HCOOH}/g_{cat}/h$ and 0.56 $mmol_{HCOOH}/g_{cat}/h$, corresponding to turnover numbers of 11 $mol_{HCOOH}/mol_{Cr}$ and 6 $mol_{HCOOH}/mol_{Ga}$, respectively. It was noteworthy that UiO-66-CAT prior to metalation as a photocatalyst did not produce HCOOH. The stability and reusability of the metalated catechol-

based MOF photocatalysts after three cycles of photocatalysis were assessed using PXRD and SEM measurements to evaluate their structural and chemical integrity.

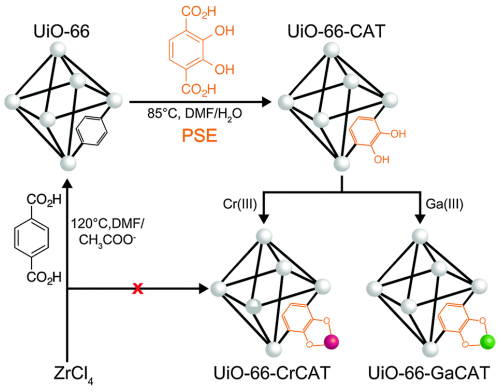


Figure 7. Synthesis of metalated catecholate-UiO-66 as $CO_2$ photoreduction catalysts. Reprinted with permission from reference 42 with permission from the Royal Society of Chemistry.

### 3.3 Metalated porphyrin linkers

Mialane, Morris, Mellot-Draznieks and coworkers explored the metalation using various cations (M = $Mn^{3+}$, $Fe^{3+}$, $Co^{2+}$, $Cu^{3+}$, $Zn^{3+}$) of the Zr-based porphyrinic MOF-545.[43] The MOF-545 was built of tetrakis(4-carboxyphenyl) porphyrin (TCPP) linkers connecting $Zr_6O_8(H_2O)_4(COOR)_8$ nodes using 1,2-dichloroacetic acid as a modulator. In this study, the synthesis of nanocrystalline MOF-545(M) was achieved via a new microwave protocol giving access to particle size of ca. 3000, 200 and 150 nm for MOF-545, NanoMOF-545 and NanoMOF-545(Fe), respectively. The activity of the MOF-545(M) series was evaluated in acetonitrile using TEOA as sacrificial electron/proton donor under visible light irradiation with a 280W Xe arc lamp. Only HCOOH was formed and no other product, such as $H_2$, CO or $CH_4$, could be observed. Amongst the MOF-545(M) series, the HCOOH production increased with the order Cu < Co < Mn < Zn < Fe, reaching a maximum of 0.57 $mmol_{HCOOH}/g_{cat}/h$ with the MOF-545(Fe) photocatalyst. In the case of

nanosized MOF catalyst, NanoMOF(Fe), the visible light-driven HCOOH production reached 1.5 $mmol_{HCOOH}/g_{cat}/h$ significantly boosted with respect to the conventional micron-sized crystals. This was attributed to an increased density of accessible catalytic sites. By combining spectroscopic and photophysical techniques with Density Functional Theory (DFT)-level calculations (Figure 8), an unconventional mechanism of the MOF-545(Fe)-catalyzed $CO_2$ photoreduction was postulated to involve (i) the photo-oxidation of TEOA at the porphyrinic linkers followed by deprotonation to yield $TEOA^{\bullet}$ radicals; (ii) the thermally-activated $CO_2$ reduction at the $Zr_6O_8(H_2O)_4(COOR)_8$ clusters using $TEOA^{\bullet}$ as hydride donor yielding to its dehydrogenated form ($ald^{\bullet}$); and (iii) the radical quenching between the reduced linker ($TCPPc^{\bullet-}$) and the dehydrogenated donor ($ald^{\bullet}$). As for UiO-type catalysts (section 2.1), the impact of leached Zr species might also play a role, in particular as the calculations were performed for isolated $Zr_6O_8(H_2O)_4(COOR)_8$ model clusters and a decrease in the crystallinity was observed after catalysis. Note that for similar isolated $Zr_6O_4(OH)_4(COOR)_{12}$ clusters the catalytic activity in $CO_2$ to CO photoreduction has been demonstrated recently.[57]

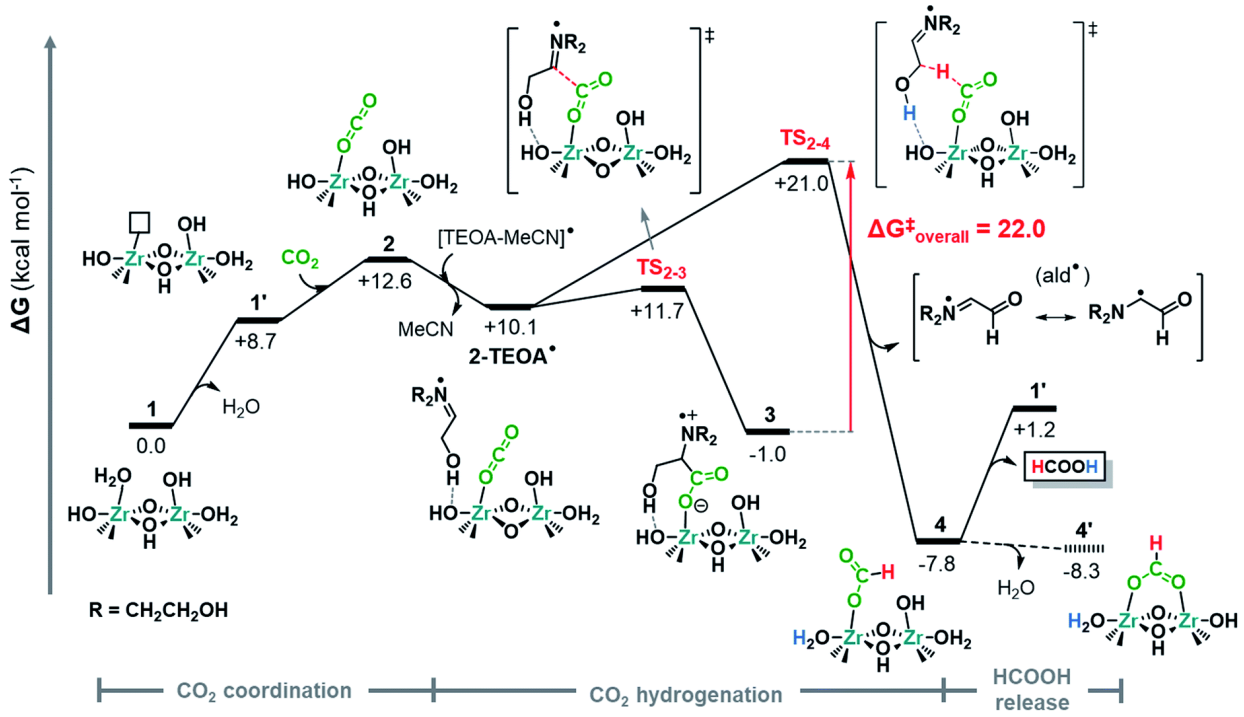


Figure 8. Gibbs free-energy profile for the reduction of $CO_2$ to HCOOH calculated for $Zr_6O_8(H_2O)_4(COOR)_8$ clusters as molecular model of the MOF-545 catalyst. Reprinted with permission from reference 43 with permission from the Royal Society of Chemistry.

Zhang, Lin and coworkers reported two new chemically stable metalloporphyrin-bridged metal-catechol frameworks able to perform $CO_2$ to HCOOH photoreduction using water instead of TEAO, BIH or BNAH as electron donor (Figure 9).[44] Theses MOF were made of metal-phenate building unit linked with photosensitive metalloporphyrins. Typically, $In(NO_3)_3$ or $FeCl_2$ reacted with 5,10,15,20-tetrakis(3,4-dihydroxyphenyl)porphyrin-Co (3,4-TDHPP-Co) to produce In/FeTCP-Co as a three-dimensional framework connected by one-dimensional indium-oxo/iron-oxo coordination rods. Similarly, In/FeTCP-OH-Co were prepared using 5,10,15,20-tetrakis(2,3,4-trihydroxyphenyl)porphyrin-Co (TCP-OH-Co) having hydroxyl moieties attached

to the 2-position of the catechol. Surface areas of InTCP-Co and FeTCP-Co reached 430 and 380 $m^2/g$, respectively, and their hydroxylated analogues InTCP-OH-Co and FeTCP-OH-Co reached 130 $m^2/g$ and 140 $m^2/g$, respectively.

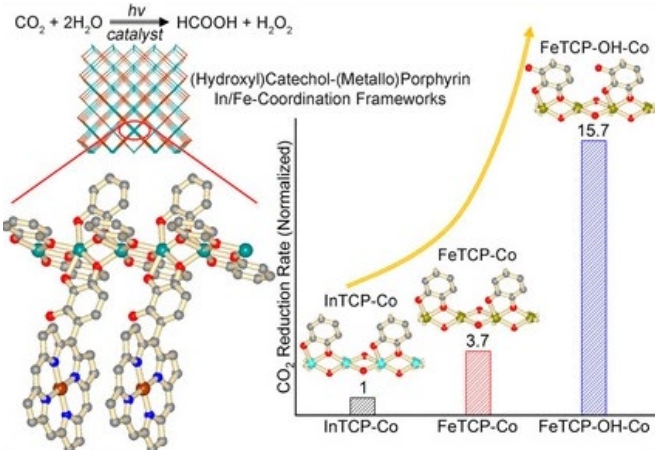


Figure 9. Metalloporphyrin-based MOF for $CO_2$ photoreduction using water instead of organic sacrificial donor. Reprinted with permission from reference 44. Copyright 2011 WILEY-VCH Verlag GmbH & Co. KGaA, Weinheim.

UV/Vis diffuse reflectance spectra (DRS) revealed that all TCP-Co-based MOF possessed excellent light absorption in the range of 200 - 800 nm. The visible-light-driven $CO_2$ reduction was performed in water without any additional sacrificial agent or photosensitizer. FeTCP-Co showed higher $CO_2$ photoreduction rate compared to InTCP-Co, and uncoordinated hydroxyl groups in TCP-OH-Co MOF was found to further promote the photocatalytic activity compared to the parent TCP-Co MOF. Indeed, HCOOH production reached 0.004 $mmol_{HCOOH}/g_{cat}/h$ for FeTCP-Co, 4-fold higher than that of InTCP-Co (0.001 $mmol_{HCOOH}/g_{cat}/h$). Similar increase in productivity was found from In to Fe in hydroxylated analogues with 0.006 $mmol_{HCOOH}/g_{cat}/h$ for InTCP-OH-Co and 0.017 $mmol_{HCOOH}/g_{cat}/h$ for FeTCP-OH-Co with 97.8% selectivity towards

HCOOH over CO as the by-product. Transient absorption (TA) and photocurrent measurements demonstrated that the iron-oxo chains and uncoordinated hydroxy groups could play dominant roles in the photogenerated charge separation and transfer. The enhancement of $CO_2$ photocatalytic performance was attributed to synergistic combination of Fe and hydroxyls groups at the catechol site giving rise to strong visible-light absorbance and appropriate energy band alignment. DFT-level calculations were also used to postulate a photoexcitation process and a photocatalytic mechanism combining $CO_2$ reduction at cobalt centers and water oxidation at the iron-catecholates to produce $H_2O_2$.

**4. Heterogenized single-site catalysts within MOF**

In contrast to the above-listed MOF-based photocatalytic systems, in the following examples the MOF only played the role of catalyst for the $CO_2$ reduction while the use of an external photosensitizer, such as ruthenium pyridyl complexes, remained necessary to the light-driven process.

**Ni/Mg-MOF-74.** Wand, Sun and coworkers reported Ni-MOF-74 and bimetallic Ni/Mg-MOF-74 with different Ni/Mg ratio.[45] MOF-74 has a honeycomb structure with one-dimensional channels of 6 Å diameter made by metal-oxo chains linked by 2,5-dihydroxy-1,4-benzenedicarboxylate linkers. The EDX analysis showed uniform distribution of Ni and Mg within the bimetallic MOF which absorbed in the whole visible light range like pure Ni-MOF-74. The $CO_2$ photoreduction was performed in an acetonitrile-triethanolamine mixture using $[Ru(bpy)_3]Cl_2$ (bpy = 2,2′-bipyridine) as the photosensitizer under visible-light irradiation (300W Xe lamp with 420 nm cutoff filter). The $Ni_{0.75}Mg_{0.25}$-MOF-74 exhibited the highest HCOOH production with a rate of 0.64 $mmol_{HCOOH}/g_{cat}/h$ which is higher than that of Ni-MOF-74 (0.29 $mmol_{HCOOH}/g_{cat}/h$). Significant CO production was reported under pure $CO_2$ atmosphere with a rate of 0.4

$mmol_{CO}/g_{cat}/h$. However, under 5% $CO_2$ atmosphere, the CO production was reduced to 0.1 $mmol_{CO}/g_{cat}/h$, four-fold lower than under pure $CO_2$, and the HCOOH production reached at 0.53 $mmol_{HCOOH}/g_{cat}/h$, corresponding to 80% of the production under pure $CO_2$. Furthermore, simulated flue gas containing $NO_x$, $H_2S$ and $SO_x$ did not alter the productivity. Such experiments are hardly provided in the literature but are of tremendous significant for the application of $CO_2$ reduction catalysts under realistic conditions, as $NO_x$, $H_2S$ and $SO_x$ represent potent catalyst poisonings. Supported by experimental $CO_2$ physisorption and photocurrent response measurements, theoretical calculations revealed that both strong binding affinity of Mg sites for $CO_2$ and lowered energy barrier for the formation of the formate radical intermediate by the cooperation of $Ni^{2+}$ and $Mg^{2+}$ were at the origin of the high HCOOH productivity.

Further strategies relayed on the use of MOF as platform for the heterogenization of molecular $CO_2$ reduction catalysts, mainly based on bipyridyl linker, and thus was envisioned as a porous macroligands, *ie* a functional porous solid acting like the organic ligand in the case of a molecular complexes.[58]

**Rh-MOP.** Furukawa and coworkers studied dinuclear Rh paddlewheels, found in molecular cages and their porous self-assemblies, in the visible-light driven $CO_2$ to HCOOH photoreduction (Figure 10).[46] The controlled arrangement of $Rh_2$ paddlewheels was reported by Furukawa and coworkers in metal-organic cages, also called metal-organic polyhedra (MOP), which are discrete molecular structures, self-assembled from bent ligands and metal precursors. The MOP $[Rh_2(bdc)_2]_{12}$ was found to self-assembled into supramolecular structures by coordination on the Rh open metal sites of 1,4-bis(imidazole-1-ylmethyl)benzene (bix) as ditopic N-donor linker, giving access to colloidal particles (Rh-CPP) or aerogels (Rh-SAG).[59,60] For comparison, they also synthesized the $Rh_3btc_2$ MOF (btc = 1,3,5-benzenetricarboxylate), an HKUST analogue made with Rh paddlewheel nodes,

first reported by Fischer and coworkers.[61] The photocatalytic $CO_2$ reduction was performed in a $CO_2$-saturated acetonitrile-TEOA solution using $Ru(bpy)_3Cl_2$ as photosensitizer and irradiation by an ABA-class solar simulator without a filter for 2 hours. The $Rh_3btc_2$ MOF catalyst showed a turnover frequency (TOF) of 5 $mol_{HCOOH}/mol_{Rh2}/h$ (10 $mmol_{HCOOH}/g_{cat}/h$). Rh-CPP and Rh-SAG showed higher catalytic activity (TOF = 56 - 59 $mol_{HCOOH}/mol_{Rh2}/h$), slightly higher than their molecular building block Rh-MOP (TOF = 45 - 52 $mol_{HCOOH}/mol_{Rh2}/h$). The significant lower activity of the $Rh_3btc_2$ MOF compared to all other catalysts was explained by a significant lower electron density on the Rh as deduced from XPS. In terms of productivity, the Rh-SAG reached 54 $mmol_{HCOOH}/g_{cat}/h$ and Rh-CPP surpassed all previous catalysts with 76 $mmol_{HCOOH}/g_{cat}/h$ using a solar simulator. Both recycling and long-term experiments highlighted the stable catalytic activity. Pair distribution function (PDF) analysis evidenced that no structural change occurred at the $Rh_2$ active site upon catalysis.

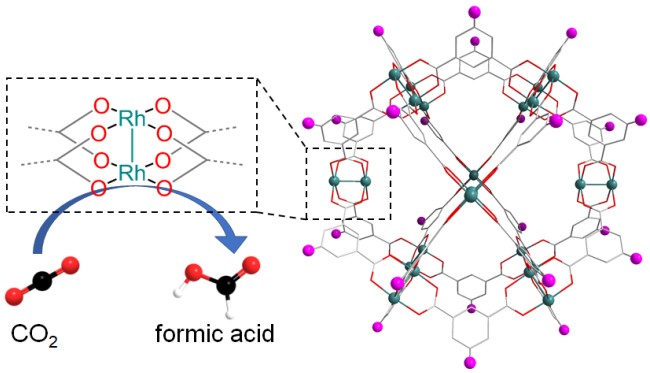


Figure 10. Rh-MOP structure as $CO_2$ photoreduction catalyst. Adapted from Ghosh *et al.*, *J. Am. Chem. Soc.* **2022**, *144* (8), 3626-3636.[46] Copyright 2022 American Chemical Society.

**Mn@UiO-67-Bpy**. Cohen and coworkers pioneered the post-synthetic metalation of robust Zr-based MOF made with open 2,2′-bipyridine metal-chelating linkers to achieve the site-isolation of $Mn(CO)_3Br$ sites in the MOF resulting in UiO-67-bpy$Mn(CO)_3Br$ catalyst.[47] The UiO-67-bpy was

prepared using an equimolar mixture of 4,4′-biphenyldicarboxylic acid and (2,2′-bipyridine)-5,5′-dicarboxylic acid with $ZrCl_4$ and acetic acid as modulator. The metalated material, UiO-67-bpyMn$(CO)_3Br$, was obtained by infiltration of $Mn(CO)_5Br$ and isolated as a red microcrystalline powder with an apparent surface area of 1430 $m^2/g$. ICP-OES and EDX analyses suggested that ca. 76% of the bpy sites were metalated. The $CO_2$ photoreduction proceeded in a DMF/TEOA solvent mixture in the presence of $[Ru(dmb)_3](PF_6)_2$ (dmb = 4,4′-dimethyl-2,2′- bipyridine) as photosensitizer and BNAH as sacrificial reducing agent under 470 nm LED irradiation (Figure 11). The UiO-67-bpyMn$(CO)_3Br$ catalyst reached a HCOOH productivity of 5 $mmol_{HCOOH}/g_{cat}/h$ and a turnover number of 110 $mol_{HCOOH}/mol_{Mn}$ after 18 h. The system produced low yields of CO and $H_2$ with TON of 4.5 and 1, respectively, after 18 h. The robust nature of the UiO-type MOF and the site-isolation inhibited the deactivation of the Mn molecular catalyst by dimerization, enabling a however limited reusability over three catalytic cycles. PXRD, FT-IR and ICP-OES data indicated that the main sources for the loss of catalytic activity were both the loss of CO ligands at the Mn sites and the slight degradation of the MOF framework.

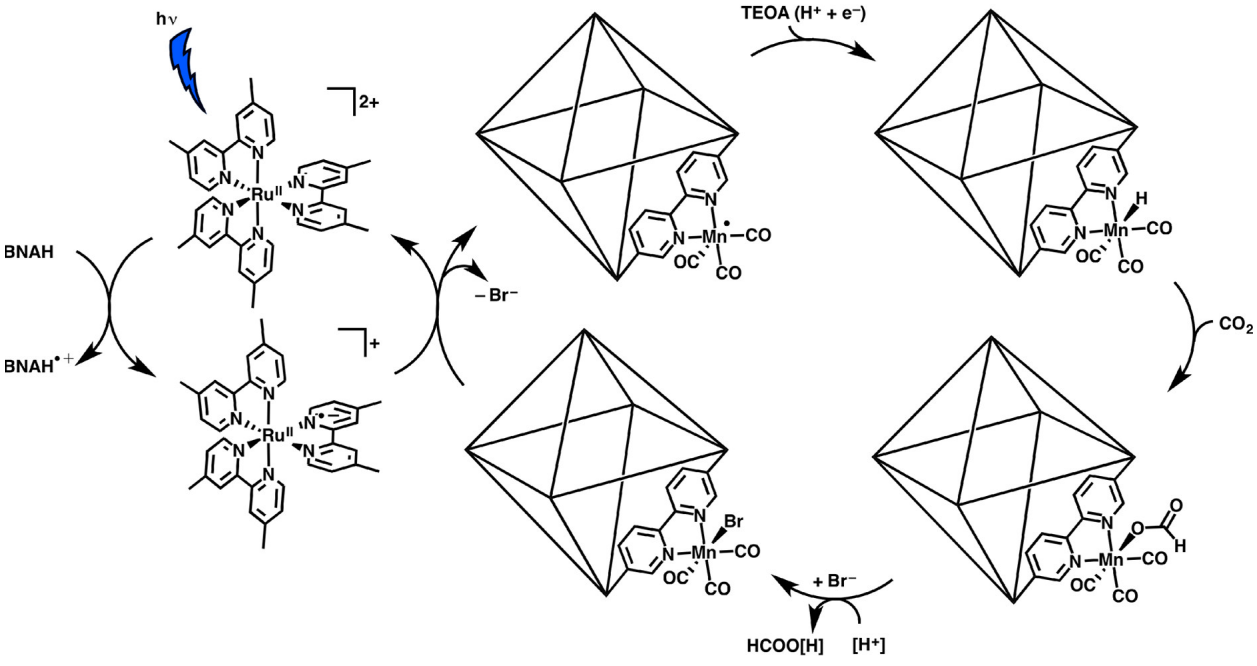

Figure 11. Proposed mechanism for the formation of HCOOH from the photocatalytic reaction with UiO-67-bpyMn(CO)$_3$Br. Reproduced from Fei *et al.*, *Inorg. Chem.* **2015**, *54* (14), 6821–6828.[47] Copyright 2015 American Chemical Society.

**Ru(terpy)@UiO-67-Bpy.** Using the same MOF hosting framework, Kitagawa and coworkers designed UiO-67 MOF functionalized with a polypyridyl ruthenium molecular catalyst.[48] From pristine UiO-67, they applied a post-synthetic linker exchange methodology using new metalated linker derivative [$Ru^{II}$($H_2$bpydc)(terpy)(CO)]($PF_6$)$_2$ ($H_2$bpydc = 2,2′-bipyridine-5,5′-dicarboxylic acid, terpy = 2,2′;6′,2″-terpyridine) to synthesized the UiO-67-bpyRu(terpy)(CO) catalyst (Figure 12). PXRD analysis of UiO-67-bpyRu(terpy)(CO) indicating the retention of the UiO-67-type framework structure during the post-synthetic linker exchange process. For a loading of 5.5 mol% of the molecular complex within the MOF framework, the apparent surface area reached 2170 $m^2$/g. Interestingly, $CO_2$ isotherms recorded at 273 and 298 K revealed an increased uptake for MOF catalyst compared to the parent UiO-67, attributed to an increase affinity for $CO_2$ upon loading with Ru(CO) species. The $CO_2$ photoreduction proceeded under visible light irradiation (385-740 nm, 67 mW/$cm^2$) in the presence of $[Ru(bpy)_3]^{2+}$ as photosensitizer and TEOA as an electron donor. HCOOH was found as the main product however with $H_2$ and CO as byproducts. The UiO-67-bpyRu(terpy)(CO) catalyst produced a larger amount of $H_2$ than its molecular counterpart suggesting that the $Zr_6O_4(OH)_4$ clusters were active as proton reduction catalysts, a side reaction however not observed for pure MOF based catalysts (see section 2.1 and 2.2). The dilution of $CO_2$ into the gaseous feed was found to impact the productivity of the molecular catalyst (TON decreased from 60 to 30 $mol_{HCOOH}/mol_{Ru(CO)}$ for 100%vol to 5%vol $CO_2$) but did not affect

that of the MOF catalyst (TON decreased from 55 to 50 $mol_{HCOOH}/mol_{Ru(CO)}$ for 100%vol to 5%vol $CO_2$), also more selective towards formic acid, reaching a productivity of 1.07 $mmol_{HCOOH}/g_{cat}/h$.

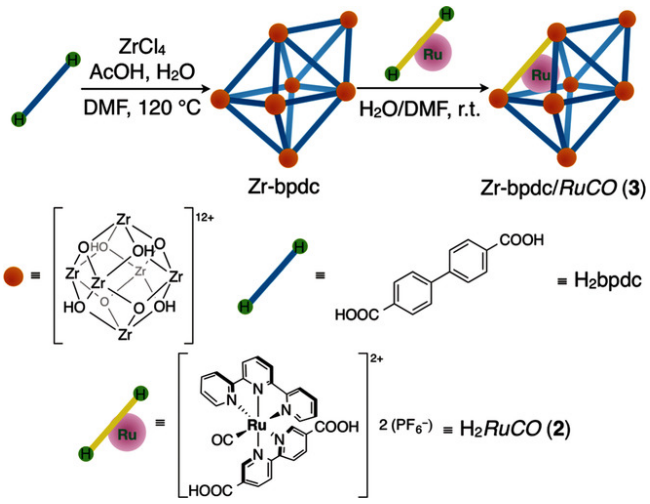


Figure 12. Synthesis of UiO-67-bpyRu(terpy)(CO) catalyst by post synthetic linker exchange. Reprinted with permission from reference 48.Copyright 2016 WILEY-VCH Verlag GmbH & Co. KGaA, Weinheim.

**Cp*Rh@UiO-67-Bpy.** Fontecave and coworkers identified a novel Rh-based selective molecular catalyst for the reduction of $CO_2$ into HCOOH and incorporated the catalyst into UiO-67 MOF as part of the framework.[49,62] Following post-synthetic ligand exchange methodology, UiO-67 reacted with the synthesized molecular complex Cp*Rh(bpydc)$Cl_2$ (Cp* = pentamethyl cyclopentadienyl) in deionized water at room temperature for 24 h (Figure 13). Ligand exchange rate varied from 5 mol% to 35 mol% with retention of the UiO-67 structure. Cp*Rh@UiO-67-bpy samples showed a linear correlation between decreased in apparent surfaces area and increased rhodium incorporation, from 1750 to 500 $m^2/g$ for 5 mol% to 35 mol% linker exchange. Photocatalytic $CO_2$ reduction reactions were performed using a mixture of acetonitrile and TEOA as both an electron and proton donor in the presence of $Ru(bpy)_3Cl_2$ as the photosensitizer. For

comparison, the molecular complexes Cp*Rh(bpy)$Cl_2$ and Cp*Rh(bpydc)$Cl_2$ were also evaluated. The two molecular catalysts showed good activity for $CO_2$ photoreduction into HCOOH under homogeneous conditions with TON of 125 $mol_{HCOOH}/mol_{Rh}$ and 42 $mol_{HCOOH}/mol_{Rh}$ for Cp*Rh(bpy)$Cl_2$ and Cp*Rh(bpydc)$Cl_2$, respectively, after 10 h reaction. $H_2$ was the only other product of the reaction with TON of 55 $mol_{H2}/mol_{Rh}$ and 38 $mol_{H2}/mol_{Rh}$ for for Cp*Rh(bpy)$Cl_2$ and Cp*Rh(bpydc)$Cl_2$, respectively, after 10 h reaction. The Cp*Rh@UiO-67-bpy heterogeneous catalyst showed TON similar to its homogeneous counterpart Cp*Rh(bpydc)$Cl_2$, including carboxylate side-groups, with TON = 47 $mol_{HCOOH}/mol_{Rh}$, corresponding to 0.3 $mmol_{HCOOH}/g_{cat}/h$, and $TON_{H2}$ = 36. Interestingly, for similar rhodium loading within catalytic system, the MOF-heterogenized catalyst was slightly more selective to HCOOH than the corresponding homogeneous counterpart.

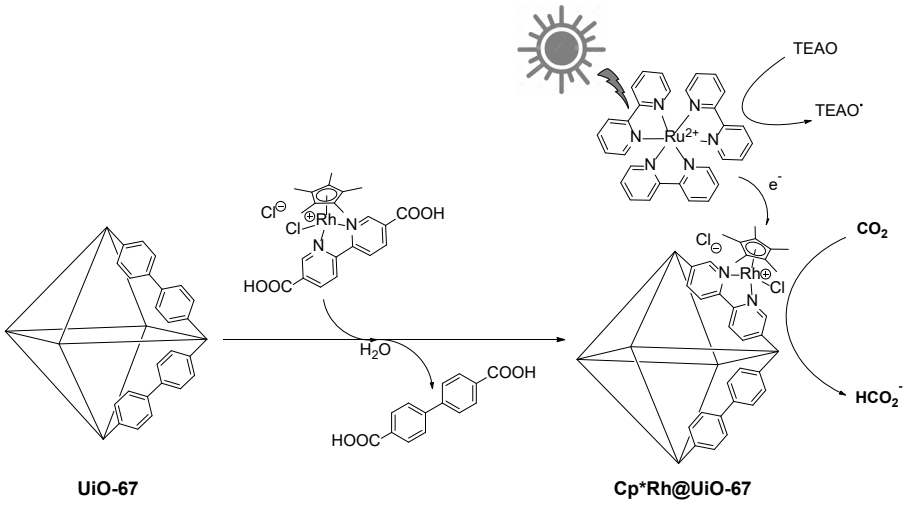


Figure 13. Synthesis of Cp*Rh@UiO-67-bpy for $CO_2$ photoreduction. Adapted from reference 49. Copyright 2015 WILEY-VCH Verlag GmbH & Co. KGaA, Weinheim.

**Cp*Rh@MOF-253 and other host materials.** Wisser, Canivet and coworkers studied the impact of different host materials on the activity of the same Cp*Rh site.[52]Also, they used a slightly different setup as Fontecave and co-workers (see Table 1), they observed similar activity for the Cp*Rh@UiO-67 catalyst. When replacing the UiO-67 host by MOF-253 (**Error! Reference source not found.Error! Reference source not found.**b), the catalytic activity drops to approx. 60% from a turnover frequency (TOF) of ~7 $h^{-1}$ (1.78 $mmol_{HCOOH}/g_{cat}/h$) to ~4 $h^{-1}$ (0.78 $mmol_{HCOOH}/g_{cat}/h$). In order to rationalize this observation, the authors designed a series of porous organic polymers (POPs) containing the 2,2′bipyridine binding site and different substituents and compared the catalytic activities of all materials to the activities for molecular model catalysts. Interestingly, the activity of the solid catalyst followed the same trend as the activity of the homogeneous model catalysts. For the latter it is well established that changes in the activity can be described by the so-called Hammett correlation. In molecular chemistry, the electronic effects of substituents are usually described using Hammett's constant, with tabulated values allowing a direct comparison of the influence at the molecular level of different functional groups on the rate of reaction. The theory shows that the electronic effects of the substituent are additive and therefore offer a wide latitude of variations. The correlation between activity and Hammett's constant in UiO-67, MOF-253 and POPs highlighted the crucial impact of the local electronic environment surrounding the active catalytic center compared to the structure on a larger scale of the porous support (porosity, dimensionality, conjugation). In this case, the POP-based catalysts showed a much smaller Hammett value compared to MOF, making them more suitable as macroligands for the Rh-catalyzed $CO_2$-to-HCOOH reduction, with TOF of up to 29 $h^{-1}$ (4.2 $mmol_{HCOOH}/g_{cat}/h$). Most importantly this correlation rules out any impact of diffusion limitation, as the material with the largest pore opening (MOF-253) showed the lowest activity.

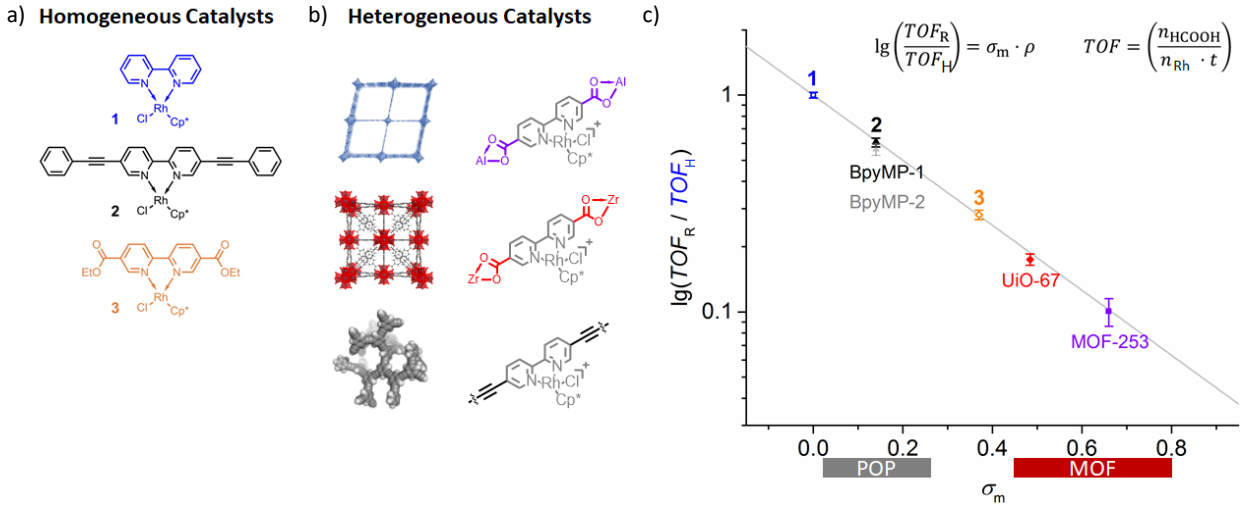


Figure 14. a) structure of molecular catalysts, b) structure of MOF and POP based catalysts and c) Structure-activity correlation bridging homogeneous and heterogenized Cp*Rh(bpy) catalysts within MOF and POP for $CO_2$ photoreduction. Adapted from Wisser *et al.*, *ACS Catal.* **2018**, *8* (3), 1653–1661.[52] Copyright 2018 American Chemical Society.

**Cp*Rh/Ru(bpy)$_3$@MIL-101.** Fontecave, Mellot-Draznieks and coworkers applied a different strategy to immobilize the same molecular active units, Cp*Rh(bpy)$Cl_2$ catalyst and Ru(bpy)$_3Cl_2$ photosensitizer derivatives, by co-encapsulation within MOF MIL-101.[50] [Ru(bpy)$_2$(4,4′-bpydc)](PF$_6$)$_2$ and [Ru(bpy)$_2$(5,5′-bpydc)](PF$_6$)$_2$ complexes were irreversibly adsorbed into Al-MIL-101-$NH_2$, structurally analogous to Cr-MIL-101 and Fe-MIL-101-$NH_2$. [Cp*Rh(4,4′-bpydc)]$Cl_2$ was similarly immobilized in the MOF. The molecular species adsorption in a 1:2 ratio into Rh–Ru@MIL-101-$NH_2$ was confirmed by inductively coupled plasma optical emission spectroscopy (ICP-OES) and liquid-state $^1$H NMR spectroscopy, with loadings of 0.61 wt% for Ru and 0.32 wt% for Rh. Porosity measurement showed a decrease in apparent surface area upon

photosystem adsorption from 2100 $m^2/g$ for the pristine Al-MIL-101-$NH_2$ to 1570 $m^2/g$ for Rh–Ru@MIL-101-$NH_2$. Finally, XPS analysis confirmed the oxidation state of the photosensitizer and the catalyst within the MOF. The photocatalytic $CO_2$ reduction was performed in a $CO_2$-saturated acetonitrile–TEOA solution under UV light irradiation with a 425 nm cut-off filter. The productivity of the Rh–Ru@MIL-101-$NH_2$ fully heterogenous photosystem reached 0.026 $mmol_{HCOOH}/g_{cat}/h$ (TON = 3 $mol_{HCOOH}/mol_{Rh}$ after 5 hours) with full selectivity for HCOOH, in contrast to the corresponding homogeneous system which gave rise to $H_2$ as major product, as well as the above discussed UiO-67 based system. The observed decrease in activity upon recycling was most likely attributed to the well-known intrinsic photodegradation of the Ru-based photosensitizer.

**$PW_{12}$/Cp*Rh@UiO-67-Bpy** Mellot-Draznieks and coworkers further studied the previous Cp*Rh@UiO-67-bpy catalytic system by exploring the potential impact of the co-immobilization of polyoxometalates (POM) and Cp*Rh catalytic complexes on the photocatalytic performances for $CO_2$ conversion.[51] The $PW_{12}$@UiO-67 composite was obtained by solvothermal self-assembly of $ZrCl_4$, $H_2$bpdc and $H_3PW_{12}O_{40}$ ($H_3PW_{12}$). Post-synthetic linker exchange with the molecular complex Cp*Rh(bpydc)$Cl_2$ yielded the ($PW_{12}$, Cp*Rh)@UiO-67. The percentage of the bpdc linkers exchanged in the MOF and the amount of POM and Rh immobilized within the UiO-67 cavities were evaluated by energy dispersive spectroscopy and elemental analyses, leading to the following proposed formula $Zr_6O_4(OH)_4(bpdc)_{5.45}(Cp^*RhCl(bpydc))_{0.44}(PW_{12}O_{40})_{0.22}$. From $^{31}P$ NMR spectroscopy, the authors suggested that two POM environments coexisted within the pristine ($PW_{12}$, Cp*Rh)@UiO-67 material, some being close to the Cp* fragment of the Cp*Rh complex and some being closer to the organic bpdc linker, also supported by DFT-level

calculations. The activity of Cp*Rh@UiO-67 and ($PW_{12}$, Cp*Rh)@UiO-67 materials were compared in an acetonitrile-TEOA mixture with $Ru(bpy)_3Cl_2$ as external photosensitizer under irradiation by a 280 W Xe lamp equipped with a 415 nm cut-off filter. After 3 hours of reaction, the productivity in $H_2$ was enhanced by a factor of 2 using (Cp*Rh, $PW_{12}$)@UiO-67 composite (0.83 $mmol_{H2}/g_{cat}/h$; TON = 20 $mol_{H2}/mol_{Rh}$) compared to the POM-free Cp*Rh@UiO-67 (0.48 $mmol_{H2}/g_{cat}/h$; TON = 7.7 $mol_{H2}/mol_{Rh}$). The production of HCOOH followed the same trend with similarly enhancement when using POM composite (0.52 $mmol_{HCOOH}/g_{cat}/h$, TON = 14 $mol_{HCOOH}/mol_{Rh}$) compared to the POM-free system (0.44 $mmol_{HCOOH}/g_{cat}/h$, TON = 7 $mol_{HCOOH}/mol_{Rh}$). The beneficial role of immobilizing POMs near catalytic sites for boosting their photocatalytic activity was later elucidated by a comprehensive approach combining DFT calculations and microkinetic modeling techniques, supplemented by photo-physical and spectroscopic experimental measurements.[63] The $PW_{12}$ POM immobilized inside the UiO-67 MOF was postulated to act as an efficient electron reservoir, accepting electrons from the photo-reduced $Ru(bpy)_3$ photosensitizer and transferring them to the Rh catalyst. The increase in $H_2$ production was attributed to concomitant increase in activity and higher concentration of protons from the reductive quenching of the photoexcited photosensitizer by TEOA.

**5. Critical assessment on parameters driving catalysis efficiency**

As mentioned in the introduction, the lack of precise information about the reactor design, the light source used (position from the reactor, constant radiant flux or irradiance) and information on the reproducibility of photocatalytic system remains a major challenge for comparing the activity in photochemical $CO_2$ reduction reaction (CRR) and thus designing better performing catalysts. As the same problems are also reported in homogeneous photochemical CRR, also the recommendation made by Beller and co-workers for homogeneous catalysis[30] should be

considered for scientist working on heterogeneous photochemical CRR alongside recommendations for classical heterogeneous photocatalysis.[64] Beside the detailed description of the reactor setup and the light source, one should consider the following points to ensure the accurate analysis of the catalytic performances obtained:

(i) Stating the number of independent experiments conducted;

(ii) Performing at least two independent measurements on independent samples;

(iii) Reporting of increased catalytic activity by reducing the catalyst loading and/or solid loading should prerequisite insurance that the reproducibility is also given at the lowest, and thus optimum, catalyst / solid loading;

(iv) Reporting quantum efficiencies for catalyst loadings within the catalyst loading of the so-called "optimal reaction rate". The optimal reaction rate is defined as the reaction rate which increases linearly with increasing catalyst/solid loading. In case the experiments are conducted with monochromatic light, an apparent optimal quantum yield might be reported.

When comparing parameters such as quantum yield, one should also consider that particle size and shape also dramatically affect light scattering, which might count for 13 to 76% loss of incoming photons in heterogeneous photocatalysis.[64,65]

For the comparison of catalytic activities considering the same active site within different MOF supports, the Hammett correlation has been demonstrated to be a useful descriptor also for heterogenized single site catalyst.[52] But such comparison is so far only feasible within one laboratory, due to the issues discussed above. However also for MOF photocatalysts with pure organic linkers (discussed in section 2) similar considerations should be considered, as De Vos, Van Speybroeck, and co-workers reported correlation between the relative rate constants of Lewis

acid catalysis in series of isostructural UiO-66 MOFs and the Hammett constant of the linker.[66,67] We would also expect an impact of the linker functionalization not only on the light harvesting capability of such MOFs (i.e., Section 2) but also on the electron density and thus on the catalytic activity of the node. Understanding those parameters will allow in the future the design of even better performing catalysts.

Another parameter which is seldom addressed in detail is the stability of the MOF under the conditions of catalysis. The often-performed powder X-ray diffraction analysis allows studying the crystalline fraction of the material. However, even if changes in the relative peak intensities, a significant increase in full width at half maximum of the peaks or a non-negligible background are observed after catalysis, the material is stated to be stable. This observation does not take into account the leaching of metal centers, which may account for a significant fraction of the catalytic activity, as demonstrated for Zr based materials by Saouma and co-workers,[34] or the formation of an amorphous phase. To this end, Taheri and Tsuzuki recently reported a detailed investigation of the photo accelerated decomposition of ZIF-8 in water.[68] Also ZIF-8 is supposed to be amongst the most stable MOFs,[69] it undergoes significant decomposition in water when irradiated with UV or near-UV visible light. The decomposition directly correlates with the absorbance spectrum of ZIF-8, underlining that formed ZnO is not responsible for the degradation.[68] In light of the work of Saouma et al. as well as Taheri and Tsuzuki it is thus recommended to perform more systematic studies on stability of the MOFs used, in particular those described in section 2, 3.1 and 3.3, as metal oxides which might be derived from decomposition of the modes such as titania are well-known photocatalysts. For systems where the MOF acts as host (section 3.2 & 4) the focus should be set on hot filtration test, that is removing the solid catalyst after a given time and conducting the reaction solely with the supernatant. If a further increase in product formation (i.e., its

concentration) is observed, leaching of catalytically active species cannot be excluded and requires further investigation. Reporting of recycling test alone is not considered to be sufficient, as the reaction might be conducted at full or equilibrium condition. In such a scenario, no reliable conclusion on the stability, recyclability and/or catalytic performance can be drawn.[70]

Understanding of the stability of MOFs under photocatalytic conditions will also be of utmost importance for designing catalytic systems which can be used in pure water or aqueous buffer solutions with water as electron and proton source. Ideally such catalysts will evolve oxygen as the sole by-product, thus avoiding the use of sacrificial electron donors (e.g. TEOA, TEA) and organic solvents (e.g. acetonitrile).[37,44] In such scenario, the full benefit of $CO_2$ reduction to convert atmospheric $CO_2$ as an urgent demand to mitigate climate change can be realized. In order to replace the sacrificial electron donors by water, however a precise understanding of the role of the amine is required. In particular as the amine might be involved in activating $CO_2$ by forming e.g. a carbamate or an hemi-ester,[71] or in the electron transfer.

## 6. Conclusions

In conclusion, the last decade has seen a tremendous evolution of hybrid heterogenous photocatalytic systems for the direct and selective light-driven production of formic acid from carbon dioxide. The design of sophisticated MOF-based and related catalysts has led to a thousand-fold increase in productivity using solar light as unique energy source. Notwithstanding the boost in activity provided by electron donors stronger than TEAO, such as BIH or BNAH, it appeared from the above-described literature that highest productivity arose from well-defined isolated noble metal sites (Ru, Rh, or Ir) within the MOF framework. In addition to potentially intrinsic catalytic site activity, the ability of MOF to favorably adsorb $CO_2$ was postulated as a key feature to reach high formic acid production. The efficient recyclability of such heterogenous catalytic

systems was mainly limited by the degradation of widely used Ru-based organometallic photosensitizer, especially for long-term reactions, which was advantageously circumvented by the use of more stable organic chromophores. The structuration of both light harvesting and catalytic units into a single framework allowed for both site-isolation and efficient charge transfer and separation at the origin of the superior stability and efficiency of MOF- and POP-based catalysts compared to analogous homogeneous systems. In the case of MOF made with photoactive linkers and/or nodes, the mechanisms at play during photocatalysis remained however often not clear or with contradicting conclusions, with a need to experimentally unravel (i) the real active site nature, in particular for materials where the node is supposed to be catalytically active, (ii) the charge transfer mechanism and (iii) the $CO_2$ activation mechanism, including also reaction intermediates. Also evidence for true heterogeneity of the catalyst including hot filtration and recycling test are often missing, but would help to understand the true nature of the catalyst. Some of these issues were addressed on the basis of molecular chemistry mechanisms in the case of heterogenized molecular catalysts. Indeed, these well-defined hybrid solid systems at the interface between homogeneous and heterogeneous catalysis represent ideal candidates for structure-activity relationship elucidation thank to the combination of computational chemistry, transient spectroscopy and advanced diffraction techniques. Furthermore, the key role of the sacrificial electron donors, in particular of triethanolamine, as unavoidable additive has been questioned and addressed under various aspects for its ability to be at the same time electron, proton or hydride donor. Albeit being used for decades, the precise role of TEOA seen in the different mechanism needs still to be elucidated.

Despite crucial advances and appealing productivities reached by the above-reviewed catalytic systems, few prerequisites remained unsolved in order to apply such systems for large-scale $CO_2$

abatement and solar fuel production. Indeed, the economic viability of these MOF-based systems might be questioned and the need to get rid of sacrificial electron donors, yielding huge amounts of organic waste without any further use, will drive the next developments in the field. Already large-scale MOF production has reached a level of maturity allowing already their application in real-life[72–75] and recent examples showed the use of MOF catalyst for the carbon dioxide-to-formic acid reaction combined with water oxidation without any sacrificial organic molecule.[37,44] Thanks to the combined effort of molecular and material science communities to tackle actual limitations, new breakthrough photosystems using MOF and related porous compounds for carbon-based solar fuels production will certainly appear in a near future.

## AUTHOR INFORMATION


### Corresponding Author

* jerome.canivet@ircelyon.univ-lyon1.fr; florian.wisser@fau.de

### ORCID

Jérôme Canivet: 0000-0002-0458-3085

Florian M. Wisser: 0000-0002-5925-895X


## ACKNOWLEDGMENT


J.C. thanks the ANR project FLIPS (ANR-21-CE07-0028) for funding.


## References

(1) Artz, J.; Müller, T. E.; Thenert, K.; Kleinekorte, J.; Meys, R.; Sternberg, A.; Bardow, A.; Leitner, W. Sustainable Conversion of Carbon Dioxide: An Integrated Review of Catalysis and Life Cycle Assessment. *Chem. Rev.* **2018**, *118* (2), 434–504. https://doi.org/10.1021/acs.chemrev.7b00435.
(2) Vooradi, R.; Anne, S. B.; Tula, A. K.; Eden, M. R.; Gani, R. Energy and $CO_2$ Management for Chemical and Related Industries: Issues, Opportunities and Challenges. *BMC Chem. Eng.* **2019**, *1* (1), 7. https://doi.org/10.1186/s42480-019-0008-6.
(3) Le, Q. V.; Nguyen, V.-H.; Nguyen, T. D.; Sharma, A.; Rahman, G.; Nguyen, D. L. T. Light-Driven Reduction of Carbon Dioxide: Altering the Reaction Pathways and Designing Photocatalysts toward Value-Added and Renewable Fuels. *Chem. Eng. Sci.* **2021**, *237*, 116547. https://doi.org/10.1016/j.ces.2021.116547.
(4) Ulmer, U.; Dingle, T.; Duchesne, P. N.; Morris, R. H.; Tavasoli, A.; Wood, T.; Ozin, G. A. Fundamentals and Applications of Photocatalytic $CO_2$ Methanation. *Nat. Commun.* **2019**, *10* (1), 3169. https://doi.org/10.1038/s41467-019-10996-2.
(5) Mura, M. G.; Luca, L. D.; Giacomelli, G.; Porcheddu, A. Formic Acid: A Promising Bio-Renewable Feedstock for Fine Chemicals. *Adv. Synth. Catal.* **2012**, *354* (17), 3180–3186. https://doi.org/10.1002/adsc.201200748.
(6) Eppinger, J.; Huang, K.-W. Formic Acid as a Hydrogen Energy Carrier. *ACS Energy Lett.* **2017**, *2* (1), 188–195. https://doi.org/10.1021/acsenergylett.6b00574.
(7) Ma, Z.; Legrand, U.; Pahija, E.; Tavares, J. R.; Boffito, D. C. From $CO_2$ to Formic Acid Fuel Cells. *Ind. Eng. Chem. Res.* **2021**, *60* (2), 803–815. https://doi.org/10.1021/acs.iecr.0c04711.
(8) Onishi, N.; Laurenczy, G.; Beller, M.; Himeda, Y. Recent Progress for Reversible Homogeneous Catalytic Hydrogen Storage in Formic Acid and in Methanol. *Coord. Chem. Rev.* **2018**, *373*, 317–332. https://doi.org/10.1016/j.ccr.2017.11.021.
(9) Cauwenbergh, R.; Das, S. Photochemical Reduction of Carbon Dioxide to Formic Acid. *Green Chem.* **2021**, *23* (7), 2553–2574. https://doi.org/10.1039/D0GC04040A.
(10) Copéret, C.; Comas-Vives, A.; Conley, M. P.; Estes, D. P.; Fedorov, A.; Mougel, V.; Nagae, H.; Núñez-Zarur, F.; Zhizhko, P. A. Surface Organometallic and Coordination Chemistry toward Single-Site Heterogeneous Catalysts: Strategies, Methods, Structures, and Activities. *Chem. Rev.* **2016**, *116* (2), 323–421. https://doi.org/10.1021/acs.chemrev.5b00373.
(11) Copéret, C.; Chabanas, M.; Petroff Saint-Arroman, R.; Basset, J.-M. Homogeneous and Heterogeneous Catalysis: Bridging the Gap through Surface Organometallic Chemistry. *Angew. Chem. Int. Ed.* **2003**, *42* (2), 156–181. https://doi.org/10.1002/anie.200390072.
(12) Copéret, C.; Fedorov, A.; Zhizhko, P. A. Surface Organometallic Chemistry: Paving the Way Beyond Well-Defined Supported Organometallics and Single-Site Catalysis. *Catal. Lett.* **2017**, *147* (9), 2247–2259. https://doi.org/10.1007/s10562-017-2107-4.
(13) Conley, M. P.; Copéret, C. State of the Art and Perspectives in the “Molecular Approach” Towards Well-Defined Heterogeneous Catalysts. *Top. Catal.* **2014**, *57* (10–13), 843–851. https://doi.org/10.1007/s11244-014-0245-0.
(14) Gao, C.; Wang, J.; Xu, H.; Xiong, Y. Coordination Chemistry in the Design of Heterogeneous Photocatalysts. *Chem. Soc. Rev.* **2017**, *46* (10), 2799–2823. https://doi.org/10.1039/c6cs00727a.
(15) Perazio, A.; Lowe, G.; Gobetto, R.; Bonin, J.; Robert, M. Light-Driven Catalytic Conversion of CO2 with Heterogenized Molecular Catalysts Based on Fourth Period Transition Metals. *Coord. Chem. Rev.* **2021**, *443*, 214018. https://doi.org/10.1016/j.ccr.2021.214018.
(16) Korzyński, M. D.; Copéret, C. Single Sites in Heterogeneous Catalysts: Separating Myth from Reality. *Trends Chem.* **2021**, *3* (10), 850–862. https://doi.org/10.1016/j.trechm.2021.07.003.
(17) Rana, P.; Kaushik, B.; Solanki, K.; Saini, K. M.; Sharma, R. K. Development of Heterogeneous Photocatalysts via the Covalent Grafting of Metal Complexes on Various Solid Supports. *Chem. Commun.* **2022**, *58* (81), 11354–11377. https://doi.org/10.1039/D2CC03568E.

(18) Morikawa, T.; Sato, S.; Sekizawa, K.; Suzuki, Tomiko. M.; Arai, T. Solar-Driven CO2 Reduction Using a Semiconductor/Molecule Hybrid Photosystem: From Photocatalysts to a Monolithic Artificial Leaf. *Acc. Chem. Res.* **2022**, *55* (7), 933–943. https://doi.org/10.1021/acs.accounts.1c00564.
(19) Jeoung, S.; Kim, S.; Kim, M.; Moon, H. R. Pore Engineering of Metal-Organic Frameworks with Coordinating Functionalities. *Coord. Chem. Rev.* **2020**, *420*, 213377. https://doi.org/10.1016/j.ccr.2020.213377.
(20) Luo, Y.-H.; Dong, L.-Z.; Liu, J.; Li, S.-L.; Lan, Y.-Q. From Molecular Metal Complex to Metal-Organic Framework: The CO2 Reduction Photocatalysts with Clear and Tunable Structure. *Coord. Chem. Rev.* **2019**, *390*, 86–126. https://doi.org/10.1016/j.ccr.2019.03.019.
(21) Bhowmik, S.; Phukan, S. J.; Sah, N. K.; Roy, M.; Garai, S.; Iyer, P. K. Review of Graphitic Carbon Nitride and Its Composite Catalysts for Selective Reduction of CO2. *ACS Appl. Nano Mater.* **2021**, *4* (12), 12845–12890. https://doi.org/10.1021/acsanm.1c02896.
(22) Zhao, G.; Huang, X.; Wang, X.; Wang, X. Progress in Catalyst Exploration for Heterogeneous CO2 Reduction and Utilization: A Critical Review. *J. Mater. Chem. A* **2017**, *5* (41), 21625–21649. https://doi.org/10.1039/C7TA07290B.
(23) Pachaiappan, R.; Rajendran, S.; Senthil Kumar, P.; Vo, D.-V. N.; K.A. Hoang, T. A Review of Recent Progress on Photocatalytic Carbon Dioxide Reduction into Sustainable Energy Products Using Carbon Nitride. *Chem. Eng. Res. Des.* **2022**, *177*, 304–320. https://doi.org/10.1016/j.cherd.2021.11.006.
(24) Lu, Q.; Eid, K.; Li, W.; Abdullah, A. M.; Xu, G.; Varma, R. S. Engineering Graphitic Carbon Nitride (g-C3N4) for Catalytic Reduction of CO2 to Fuels and Chemicals: Strategy and Mechanism. *Green Chem.* **2021**, *23* (15), 5394–5428. https://doi.org/10.1039/D1GC01303C.
(25) Dhakshinamoorthy, A.; Asiri, A. M.; García, H. Metal–Organic Framework (MOF) Compounds: Photocatalysts for Redox Reactions and Solar Fuel Production. *Angew. Chem. Int. Ed.* **2016**, *55* (18), 5414–5445. https://doi.org/10.1002/anie.201505581.
(26) Li, R.; Zhang, W.; Zhou, K. Metal-Organic-Framework-Based Catalysts for Photoreduction of CO2. *Adv. Mater.* **2018**, *30* (35), 1705512. https://doi.org/10.1002/adma.201705512.
(27) Ezugwu, C. I.; Liu, S.; Li, C.; Zhuiykov, S.; Roy, S.; Verpoort, F. Engineering Metal-Organic Frameworks for Efficient Photocatalytic Conversion of CO2 into Solar Fuels. *Coord. Chem. Rev.* **2022**, *450*, 214245. https://doi.org/10.1016/j.ccr.2021.214245.
(28) Luo, T.; Wang, Z.; Han, X.; Chen, Y.; Iuga, D.; Lee, D.; An, B.; Xu, S.; Kang, X.; Tuna, F.; McInnes, E. J. L.; Hughes, L.; Spencer, B. F.; Schr, öder M.; Yang, S. Efficient Photocatalytic Reduction of CO2 Catalyzed by the Metal–Organic Framework MFM-300(Ga). *CCS Chem.* **2022**, *4* (8), 2560–2569. https://doi.org/10.31635/ccschem.022.202201931.
(29) Martín-Sómer, M.; Pablos, C.; van Grieken, R.; Marugán, J. Influence of Light Distribution on the Performance of Photocatalytic Reactors: LED vs Mercury Lamps. *Appl. Catal. B Environ.* **2017**, *215*, 1–7. https://doi.org/10.1016/j.apcatb.2017.05.048.
(30) Marx, M.; Mele, A.; Spannenberg, A.; Steinlechner, C.; Junge, H.; Schollhammer, P.; Beller, M. Addressing the Reproducibility of Photocatalytic Carbon Dioxide Reduction. *ChemCatChem* **2020**, *12* (6), 1603–1608. https://doi.org/10.1002/cctc.201901686.
(31) Fu, Y.; Sun, D.; Chen, Y.; Huang, R.; Ding, Z.; Fu, X.; Li, Z. An Amine-Functionalized Titanium Metal-Organic Framework Photocatalyst with Visible-Light-Induced Activity for $CO_2$ Reduction. *Angew. Chem. Int. Ed.* **2012**, *51* (14), 3364–3367. https://doi.org/10.1002/anie.201108357.
(32) Sun, D.; Fu, Y.; Liu, W.; Ye, L.; Wang, D.; Yang, L.; Fu, X.; Li, Z. Studies on Photocatalytic $CO_2$ Reduction over $NH_2$-Uio-66(Zr) and Its Derivatives: Towards a Better Understanding of Photocatalysis on Metal-Organic Frameworks. *Chem. - Eur. J.* **2013**, *19* (42), 14279–14285. https://doi.org/10.1002/chem.201301728.

(33) Sun, M.; Yan, S.; Sun, Y.; Yang, X.; Guo, Z.; Du, J.; Chen, D.; Chen, P.; Xing, H. Enhancement of Visible-Light-Driven $CO_2$ Reduction Performance Using an Amine-Functionalized Zirconium Metal–Organic Framework. *Dalton Trans.* **2018**, *47* (3), 909–915. https://doi.org/10.1039/C7DT04062H.
(34) Bhattacharya, M.; Chandler, K. J.; Geary, J.; Saouma, C. T. The Role of Leached Zr in the Photocatalytic Reduction of CO2 to Formate by Derivatives of UiO-66 Metal Organic Frameworks. *Dalton Trans.* **2020**, *49* (15), 4751–4757. https://doi.org/10.1039/D0DT00524J.
(35) Wang, D.; Huang, R.; Liu, W.; Sun, D.; Li, Z. Fe-Based MOFs for Photocatalytic $CO_2$ Reduction: Role of Coordination Unsaturated Sites and Dual Excitation Pathways. *ACS Catal.* **2014**, *4* (12), 4254–4260. https://doi.org/10.1021/cs501169t.
(36) Sun, D.; Liu, W.; Fu, Y.; Fang, Z.; Sun, F.; Fu, X.; Zhang, Y.; Li, Z. Noble Metals Can Have Different Effects on Photocatalysis Over Metal-Organic Frameworks (MOFs): A Case Study on M/$NH_2$-MIL-125(Ti) (M=Pt and Au). *Chem. - Eur. J.* **2014**, *20* (16), 4780–4788. https://doi.org/10.1002/chem.201304067.
(37) Hao, Y.-C.; Chen, L.-W.; Li, J.; Guo, Y.; Su, X.; Shu, M.; Zhang, Q.; Gao, W.-Y.; Li, S.; Yu, Z.-L.; Gu, L.; Feng, X.; Yin, A.-X.; Si, R.; Zhang, Y.-W.; Wang, B.; Yan, C.-H. Metal-Organic Framework Membranes with Single-Atomic Centers for Photocatalytic $CO_2$ and $O_2$ Reduction. *Nat. Commun.* **2021**, *12* (1), 2682. https://doi.org/10.1038/s41467-021-22991-7.
(38) Dai, S.; Kajiwara, T.; Ikeda, M.; Romero-Muñiz, I.; Patriarche, G.; Platero-Prats, A. E.; Vimont, A.; Daturi, M.; Tissot, A.; Xu, Q.; Serre, C. Ultrasmall Copper Nanoclusters in Zirconium Metal-Organic Frameworks for the Photoreduction of CO2. *Angew. Chem. Int. Ed.* **2022**, e202211848. https://doi.org/10.1002/anie.202211848.
(39) Kamakura, Y.; Yasuda, S.; Hosokawa, N.; Nishioka, S.; Hongo, S.; Yokoi, T.; Tanaka, D.; Maeda, K. Selective $CO_2$-to-Formate Conversion Driven by Visible Light over a Precious-Metal-Free Nonporous Coordination Polymer. *ACS Catal.* **2022**, *12* (16), 10172–10178. https://doi.org/10.1021/acscatal.2c02177.
(40) Li, L.; Zhang, S.; Xu, L.; Wang, J.; Shi, L.-X.; Chen, Z.-N.; Hong, M.; Luo, J. Effective Visible-Light Driven CO2 Photoreduction via a Promising Bifunctional Iridium Coordination Polymer. *Chem. Sci.* **2014**, *5* (10), 3808–3813. https://doi.org/10.1039/C4SC00940A.
(41) Zhang, S.; Li, L.; Zhao, S.; Sun, Z.; Hong, M.; Luo, J. Hierarchical Metal–Organic Framework Nanoflowers for Effective $CO_2$ Transformation Driven by Visible Light. *J. Mater. Chem. A* **2015**, *3* (30), 15764–15768. https://doi.org/10.1039/C5TA03322E.
(42) Lee, Y.; Kim, S.; Fei, H.; Kang, J. K.; Cohen, S. M. Photocatalytic $CO_2$ Reduction Using Visible Light by Metal-Monocatecholato Species in a Metal–Organic Framework. *Chem. Commun.* **2015**, *51* (92), 16549–16552. https://doi.org/10.1039/C5CC04506A.
(43) Benseghir, Y.; Solé-Daura, A.; Cairnie, D. R.; Robinson, A. L.; Duguet, M.; Mialane, P.; Gairola, P.; Gomez-Mingot, M.; Fontecave, M.; Iovan, D.; Bonnett, B.; Morris, A. J.; Dolbecq, A.; Mellot-Draznieks, C. Unveiling the Mechanism of the Photocatalytic Reduction of $CO_2$ to Formate Promoted by Porphyrinic Zr-Based Metal–Organic Frameworks. *J. Mater. Chem. A* **2022**, *10* (35), 18103–18115. https://doi.org/10.1039/D2TA04164B.
(44) Chen, E.-X.; Qiu, M.; Zhang, Y.-F.; He, L.; Sun, Y.-Y.; Zheng, H.-L.; Wu, X.; Zhang, J.; Lin, Q. Energy Band Alignment and Redox-Active Sites in Metalloporphyrin-Spaced Metal-Catechol Frameworks for Enhanced CO2 Photoreduction. *Angew. Chem. Int. Ed.* **2022**, *61* (1), e202111622. https://doi.org/10.1002/anie.202111622.
(45) Guo, S.-H.; Qi, X.-J.; Zhou, H.-M.; Zhou, J.; Wang, X.-H.; Dong, M.; Zhao, X.; Sun, C.-Y.; Wang, X.-L.; Su, Z.-M. A Bimetallic-MOF Catalyst for Efficient $CO_2$ Photoreduction from Simulated Flue Gas to Value-Added Formate. *J. Mater. Chem. A* **2020**, *8* (23), 11712–11718. https://doi.org/10.1039/D0TA00205D.

(46) Ghosh, A. C.; Legrand, A.; Rajapaksha, R.; Craig, G. A.; Sassoye, C.; Balázs, G.; Farrusseng, D.; Furukawa, S.; Canivet, J.; Wisser, F. M. Rhodium-Based Metal–Organic Polyhedra Assemblies for Selective CO2 Photoreduction. *J. Am. Chem. Soc.* **2022**, *144* (8), 3626–3636. https://doi.org/10.1021/jacs.1c12631.
(47) Fei, H.; Sampson, M. D.; Lee, Y.; Kubiak, C. P.; Cohen, S. M. Photocatalytic $CO_2$ Reduction to Formate Using a Mn(I) Molecular Catalyst in a Robust Metal–Organic Framework. *Inorg. Chem.* **2015**, *54* (14), 6821–6828. https://doi.org/10.1021/acs.inorgchem.5b00752.
(48) Kajiwara, T.; Fujii, M.; Tsujimoto, M.; Kobayashi, K.; Higuchi, M.; Tanaka, K.; Kitagawa, S. Photochemical Reduction of Low Concentrations of $CO_2$ in a Porous Coordination Polymer with a Ruthenium(II)–CO Complex. *Angew. Chem. Int. Ed.* **2016**, *55* (8), 2697–2700. https://doi.org/10.1002/anie.201508941.
(49) Chambers, M. B.; Wang, X.; Elgrishi, N.; Hendon, C. H.; Walsh, A.; Bonnefoy, J.; Canivet, J.; Quadrelli, E. A.; Farrusseng, D.; Mellot-Draznieks, C.; Fontecave, M. Photocatalytic Carbon Dioxide Reduction with Rhodium-Based Catalysts in Solution and Heterogenized within Metal-Organic Frameworks. *ChemSusChem* **2015**, *8* (4), 603–608. https://doi.org/10.1002/cssc.201403345.
(50) Wang, X.; Wisser, F. M.; Canivet, J.; Fontecave, M.; Mellot-Draznieks, C. Immobilization of a Full Photosystem in the Large-Pore MIL-101 Metal–Organic Framework for CO2 Reduction. *ChemSusChem* **2018**, *0* (0). https://doi.org/10.1002/cssc.201801066.
(51) Benseghir, Y.; Lemarchand, A.; Duguet, M.; Mialane, P.; Gomez-Mingot, M.; Roch-Marchal, C.; Pino, T.; Ha-Thi, M.-H.; Haouas, M.; Fontecave, M.; Dolbecq, A.; Sassoye, C.; Mellot-Draznieks, C. Co-Immobilization of a Rh Catalyst and a Keggin Polyoxometalate in the UiO-67 Zr-Based Metal–Organic Framework: In Depth Structural Characterization and Photocatalytic Properties for $CO_2$ Reduction. *J. Am. Chem. Soc.* **2020**, *142* (20), 9428–9438. https://doi.org/10.1021/jacs.0c02425.
(52) Wisser, F. M.; Berruyer, P.; Cardenas, L.; Mohr, Y.; Quadrelli, E. A.; Lesage, A.; Farrusseng, D.; Canivet, J. Hammett Parameter in Microporous Solids as Macroligands for Heterogenized Photocatalysts. *ACS Catal.* **2018**, *8* (3), 1653–1661. https://doi.org/10.1021/acscatal.7b03998.
(53) Dan-Hardi, M.; Serre, C.; Frot, T.; Rozes, L.; Maurin, G.; Sanchez, C.; Férey, G. A New Photoactive Crystalline Highly Porous Titanium(IV) Dicarboxylate. *J. Am. Chem. Soc.* **2009**, *131* (31), 10857–10859. https://doi.org/10.1021/ja903726m.
(54) Kameneva, O.; Kuznestov, A. I.; Smirnova, L. A.; Rozes, L.; Sanchez, C.; Alexandrov, A.; Bityurin, N.; Chhor, K.; Kanaev, A. New Photoactive Hybrid Organic–Inorganic Materials Based on Titanium-Oxo-PHEMA Nanocomposites Exhibiting Mixed Valence Properties. *J. Mater. Chem.* **2005**, *15* (33), 3380–3383. https://doi.org/10.1039/B507305G.
(55) Hendon, C. H.; Tiana, D.; Fontecave, M.; Sanchez, C.; D'arras, L.; Sassoye, C.; Rozes, L.; Mellot-Draznieks, C.; Walsh, A. Engineering the Optical Response of the Titanium-MIL-125 Metal–Organic Framework through Ligand Functionalization. *J. Am. Chem. Soc.* **2013**, *135* (30), 10942–10945. https://doi.org/10.1021/ja405350u.
(56) Naeem, A.; Ting, V. P.; Hintermair, U.; Tian, M.; Telford, R.; Halim, S.; Nowell, H.; Hołyńska, M.; Teat, S. J.; Scowen, I. J.; Nayak, S. Mixed-Linker Approach in Designing Porous Zirconium-Based Metal–Organic Frameworks with High Hydrogen Storage Capacity. *Chem. Commun.* **2016**, *52* (50), 7826–7829. https://doi.org/10.1039/C6CC03787A.
(57) Tan, L.; Li, Y.; Lv, Q.; Gan, Y.; Fang, Y.; Tang, Y.; Wu, L.; Fang, Y. Development of Soluble UiO-66 to Improve Photocatalytic CO2 Reduction. *Catal. Today* **2022**. https://doi.org/10.1016/j.cattod.2022.05.001.
(58) Wisser, F. M.; Mohr, Y.; Quadrelli, E. A.; Canivet, J. Porous Macroligands: Materials for Heterogeneous Molecular Catalysis. *ChemCatChem* **2020**, *12* (5), 1270–1275. https://doi.org/10.1002/cctc.201902064.

(59) Wang, Z.; Santos, C. V.; Legrand, A.; Haase, F.; Hara, Y.; Kanamori, K.; Aoyama, T.; Urayama, K.; Doherty, C. M.; Smales, G. J.; Pauw, B. R.; Colón, Y. J.; Furukawa, S. Multiscale Structural Control of Linked Metal–Organic Polyhedra Gel by Aging-Induced Linkage-Reorganization. *Chem. Sci.* **2021**, *12* (38), 12556–12563. https://doi.org/10.1039/D1SC02883A.
(60) Legrand, A.; Craig, G. A.; Bonneau, M.; Minami, S.; Urayama, K.; Furukawa, S. Understanding the Multiscale Self-Assembly of Metal–Organic Polyhedra towards Functionally Graded Porous Gels. *Chem. Sci.* **2019**, *10* (47), 10833–10842. https://doi.org/10.1039/C9SC04543K.
(61) Heinz, W. R.; Kratky, T.; Drees, M.; Wimmer, A.; Tomanec, O.; Günther, S.; Schuster, M.; Fischer, R. A. Mixed Precious-Group Metal–Organic Frameworks: A Case Study of the HKUST-1 Analogue [RuxRh3−x(BTC)2]. *Dalton Trans.* **2019**, *48* (32), 12031–12039. https://doi.org/10.1039/C9DT01198F.
(62) Hendon, C. H.; Bonnefoy, J.; Quadrelli, E. A.; Canivet, J.; Chambers, M. B.; Rousse, G.; Walsh, A.; Fontecave, M.; Mellot-Draznieks, C. A Simple and Non-Destructive Method for Assessing the Incorporation of Bipyridine Dicarboxylates as Linkers within Metal-Organic Frameworks. *Chem.-Eur. J.* **2016**, *22* (11), 3713–3718. https://doi.org/10.1002/chem.201600143.
(63) Solé-Daura, A.; Benseghir, Y.; Ha-Thi, M.-H.; Fontecave, M.; Mialane, P.; Dolbecq, A.; Mellot-Draznieks, C. Origin of the Boosting Effect of Polyoxometalates in Photocatalysis: The Case of $CO_2$ Reduction by a Rh-Containing Metal–Organic Framework. *ACS Catal.* **2022**, *12* (15), 9244–9255. https://doi.org/10.1021/acscatal.2c02088.
(64) Kisch, H.; Bahnemann, D. Best Practice in Photocatalysis: Comparing Rates or Apparent Quantum Yields? *J. Phys. Chem. Lett.* **2015**, *6* (10), 1907–1910. https://doi.org/10.1021/acs.jpclett.5b00521.
(65) Kisch, H. On the Problem of Comparing Rates or Apparent Quantum Yields in Heterogeneous Photocatalysis. *Angew. Chem. Int. Ed.* **2010**, *49* (50), 9588–9589. https://doi.org/10.1002/anie.201002653.
(66) Vermoortele, F.; Vandichel, M.; Van de Voorde, B.; Ameloot, R.; Waroquier, M.; Van Speybroeck, V.; De Vos, D. E. Electronic Effects of Linker Substitution on Lewis Acid Catalysis with Metal–Organic Frameworks. *Angew. Chem. Int. Ed.* **2012**, *51* (20), 4887–4890. https://doi.org/10.1002/anie.201108565.
(67) Vandichel, M.; Hajek, J.; Vermoortele, F.; Waroquier, M.; Vos, D. E. D.; Speybroeck, V. V. Active Site Engineering in UiO-66 Type Metal–Organic Frameworks by Intentional Creation of Defects: A Theoretical Rationalization. *CrystEngComm* **2014**, *17* (2), 395–406. https://doi.org/10.1039/C4CE01672F.
(68) Taheri, M.; Tsuzuki, T. Photo-Accelerated Hydrolysis of Metal Organic Framework ZIF-8. *ACS Mater. Lett.* **2021**, *3* (2), 255–260. https://doi.org/10.1021/acsmaterialslett.0c00522.
(69) Park, K. S.; Ni, Z.; Côté, A. P.; Choi, J. Y.; Huang, R.; Uribe-Romo, F. J.; Chae, H. K.; O'Keeffe, M.; Yaghi, O. M. Exceptional Chemical and Thermal Stability of Zeolitic Imidazolate Frameworks. *Proc. Natl. Acad. Sci.* **2006**, *103* (27), 10186–10191. https://doi.org/10.1073/pnas.0602439103.
(70) Kramm, U. I.; Marschall, R.; Rose, M. Pitfalls in Heterogeneous Thermal, Electro- and Photocatalysis. *ChemCatChem* **2019**, *11* (11), 2563–2574. https://doi.org/10.1002/cctc.201900137.
(71) Sampaio, R. N.; Grills, D. C.; Polyansky, D. E.; Szalda, D. J.; Fujita, E. Unexpected Roles of Triethanolamine in the Photochemical Reduction of CO2 to Formate by Ruthenium Complexes. *J. Am. Chem. Soc.* **2020**, *142* (5), 2413–2428. https://doi.org/10.1021/jacs.9b11897.
(72) Cordova, K. E.; Yaghi, O. M. The 'Folklore' and Reality of Reticular Chemistry. *Mater. Chem. Front.* **2017**, *1* (7), 1304–1309. https://doi.org/10.1039/C7QM00144D.
(73) Schoedel, A.; Ji, Z.; Yaghi, O. M. The Role of Metal–Organic Frameworks in a Carbon-Neutral Energy Cycle. *Nat. Energy* **2016**, *1* (4), 1–13. https://doi.org/10.1038/nenergy.2016.34.

(74) Almassad, H. A.; Abaza, R. I.; Siwwan, L.; Al-Maythalony, B.; Cordova, K. E. Environmentally Adaptive MOF-Based Device Enables Continuous Self-Optimizing Atmospheric Water Harvesting. *Nat. Commun.* **2022**, *13* (1), 4873. https://doi.org/10.1038/s41467-022-32642-0.
(75) Frameworks for Commercial Success. *Nat. Chem.* **2016**, *8* (11), 987–987. https://doi.org/10.1038/nchem.2661.